

Review

Corrosion and Wear Behavior of Additively Manufactured Metallic Parts in Biomedical Applications

Zhongbin Wei ¹, Shokouh Attarilar ², Mahmoud Ebrahimi ^{3,*} and Jun Li ⁴

- ¹ School of Mechanical Engineering, Xijing University, Xi'an 710123, China; zhongbinwei@xijing.edu.cn
² National Engineering Research Center of Light Alloy Net Forming and Key State Laboratory of Metal Matrix Composites, School of Material Science and Engineering, Shanghai Jiao Tong University, Shanghai 200240, China; sh.attarilar@yahoo.com
³ Department of Mechanical Engineering, Faculty of Engineering, University of Maragheh, Maragheh P.O. Box 55136-533, Iran
⁴ School of Physics and Materials Science, Guangzhou University, Guangzhou 510006, China; lijun0724@gzhu.edu.cn
* Correspondence: ebrahimi@maragheh.ac.ir; Tel.: +98-914-401-7268

Abstract: Today, parts made by additive manufacturing (AM) methods have found many applications in the medical industry, the main reasons for which are the ability to custom design and manufacture complex structures, their short production cycle, their ease of utilization, and on-site fabrication, leading to the fabrication of next-generation intricate patient-specific biomedical implants. These parts should fulfill numerous requirements, such as having acceptable mechanical strength, biocompatibility, satisfactory surface characteristics, and excellent corrosion and wear performance. It was known that AM techniques may lead to some uncertainties influencing part properties and causing significant evaluation conflicts in corrosion outcomes. Meanwhile, the corrosion and wear behavior of additively manufactured materials are not comprehensively discussed. In this regard, the present work is a review of the state-of-the-art knowledge dedicated to reviewing the actual scientific knowledge about the corrosion and wear response of additively manufactured biomedical components, elucidating the relevant mechanism and influential factors to enhance the performance of AM-manufactured implants specifically for the physiological human body fluids. Furthermore, there is a focus on the use of reinforced composites, surface engineering, and a preparation stage that can considerably affect the tribocorrosion behavior of AM-produced parts. The improvement of tribocorrosion performance can have a key role in the production of advanced AM implants and the present study can pave the way toward facile production of high-throughput AM biomedical parts that have very high resistance to corrosion and wear.

Keywords: 3D printing; additive manufacturing; tribocorrosion; wear; corrosion; biomedical implants



Citation: Wei, Z.; Attarilar, S.; Ebrahimi, M.; Li, J. Corrosion and Wear Behavior of Additively Manufactured Metallic Parts in Biomedical Applications. *Metals* **2024**, *14*, 96. <https://doi.org/10.3390/met14010096>

Academic Editor: Amir Mostafaei

Received: 8 December 2023

Revised: 1 January 2024

Accepted: 11 January 2024

Published: 13 January 2024



Copyright: © 2024 by the authors. Licensee MDPI, Basel, Switzerland. This article is an open access article distributed under the terms and conditions of the Creative Commons Attribution (CC BY) license (<https://creativecommons.org/licenses/by/4.0/>).

1. Introduction

Recently, additive manufacturing (AM) technologies as an emerging and attractive digital fabrication procedure have become a favorite option for biomedical applications and implant design, mostly due to their many beneficial aspects in comparison to conventional methods. These beneficial aspects of AM methods include a fast production process; on-site fabrication; precise control over dimensions, shape, and texture; their exceptional capability to produce intricate and complex-shaped structures; their ability to use pre-designed computer models; and offering cost-effective customized solutions according to patient's needs [1,2]. As shown in Figure 1, numerous AM techniques also known as three-dimensional (3D) printing methods with seven main categories that are classified according to the material addition mode and a working mechanism were introduced and implemented [3]. The suitable method for the fabrication of metallic bioimplants should

be chosen considering the type of material (metal, plastic, alloys, ceramics, wax), the state of the material (powder, liquid, wire, etc.), type of consolidation (sintering, polymerizing, fusing, laser melting, UV curing, etc.), and printing speed [4]. For the specific case of metallic bioimplants, powder bed fusion or melting techniques are usually utilized under which electron beam melting (EBM) and selective laser melting (SLM) are the most favored methods. During powder bed fusion techniques (SLS, EBM, polymer laser sintering, direct metal laser sintering, and SLM), a thermal source (laser or electron beam) is used to selectively melt/fuse the material that is held in a tray. Then, the melted/fused materials are consecutively printed in a layer-by-layer manner [5,6]; Figure 2 schematically exhibits the laser powder bed fusion device and process.

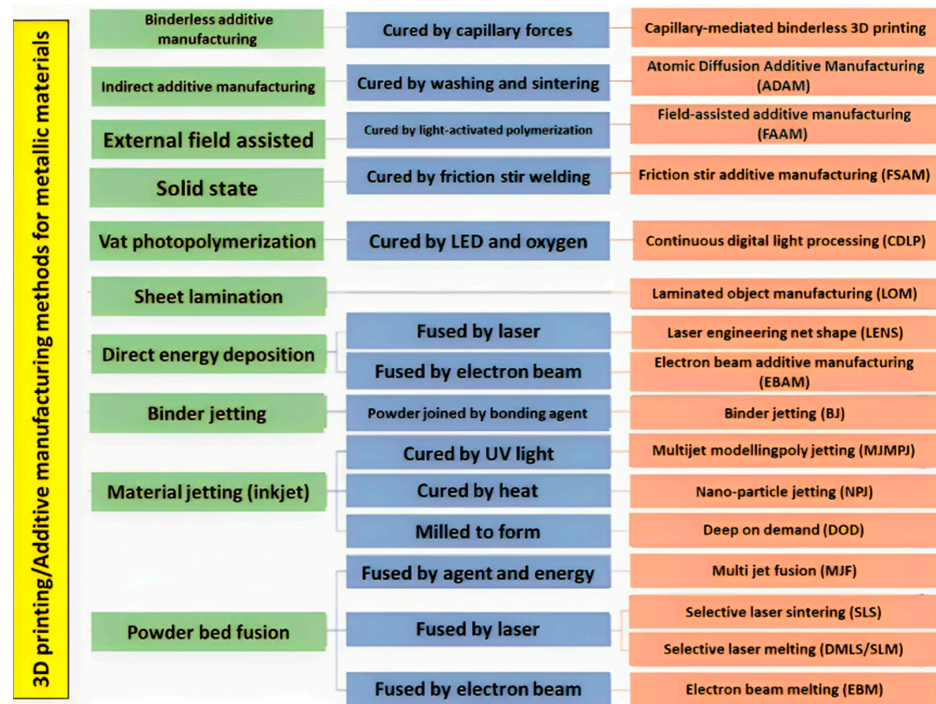


Figure 1. The main AM and 3D printing technologies for metallic materials are classified according to the material addition mode and working mechanism.

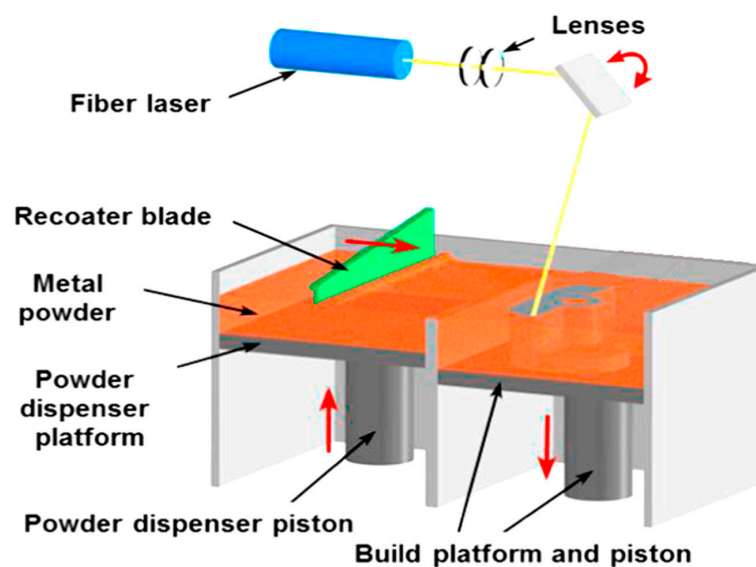


Figure 2. The laser powder bed fusion device and process. Reprinted with permission from Ref. [7]. Copyright 2017 Elsevier.

It was reported that until 2019, close to 13% of annual AM revenues directly arrived from the biomedical industry and now it is expanding at an increasing speed. The utilization of AM techniques provides the possibility for experts in this field to design customized patient-specific bioimplants and devices with exceptionally high resolutions even up to nanometric ranges at an affordable cost; some of the different kinds of used metallic implants and AM-manufactured metallic implants are shown in Figure 3. Moreover, AM products can easily undergo sterilization procedures during production and post-production steps. Therefore, the AM-manufactured parts found numerous versatile applications in the biomedical industry, including use as joint replacements, surgical implants, artificial limbs, bone and dental implants, bone fixations, hearing aids, heart valves, osteosynthesis devices, mid-facial fracture treatment, etc. [8–19]. Despite the mentioned advantageous aspects of AM-produced parts, unfortunately, they also have some limitations, such as shrinkage issues due to heat effects, thermal damages, cracks, microfractures, voids, the presence of porosity, etc., and it should be noted that some of the AM methods need post-processing stages limiting their utilization, some have low processing speed and resolution, and some have a toxic nature [9,20–25]. Other issues with AM products are related to their corrosion and wear performance, or in other words their tribocorrosion behavior, that is induced by the tribological and electrochemical variation of the material due to the presence of voids, pores, molten pool boundaries, surface roughness, and anisotropy. These properties are of crucial importance in the biomedical field since the low wear and corrosion performance may lead to the release of toxic/allergic elements and particles in the periphery of the implant, bacterial inflammation, and finally the loosening and failure of the implant that necessitates second surgeries, incurring a low quality of life and economic costs for patients [26–33].

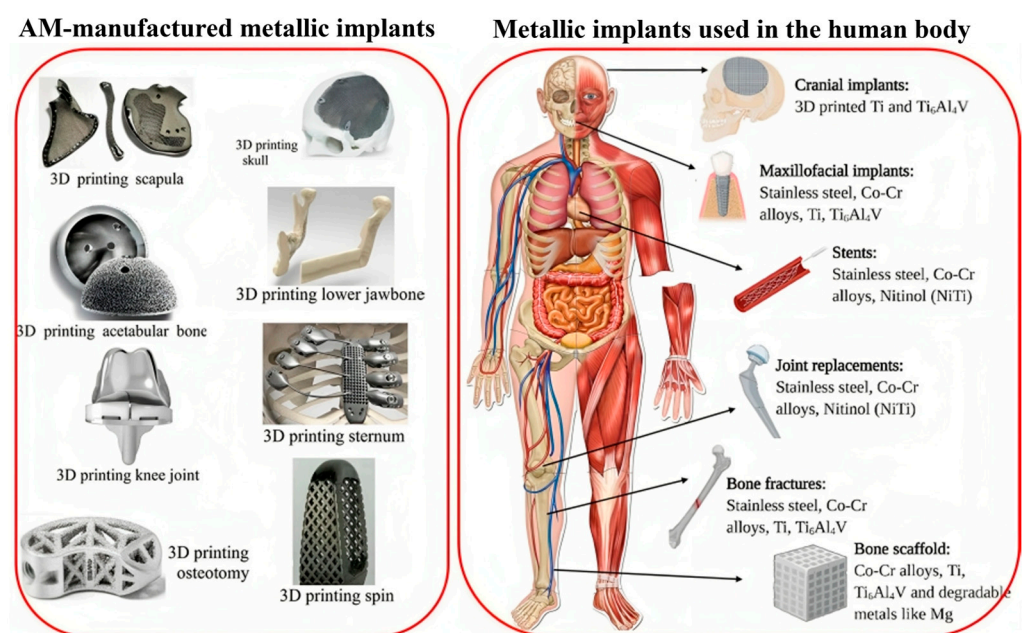


Figure 3. The different kinds of used metallic implants and the AM-manufactured metallic implants.

It has been established that additive manufacturing can significantly change the electrochemical and tribological responses of materials. Therefore, it is of utmost importance to study the influence of different parameters and associated mechanisms. Meanwhile, the microstructure also plays a key role, and its refinement due to fast melting and solidification can change the electrochemical response and reduce the wear rate. In fact, many variables should be considered to reach an in-depth and precise view of the role of AM manufacturing and its effects on wear and corrosion. The study of the corrosion and wear behavior of additively manufactured metal parts in biomedical applications is crucial for the development of safe and reliable biomedical implants. While there have been several

studies on the topic, there are still some critical comments and shortcomings that need to be addressed. For instance, some studies have focused on the corrosion and wear behavior of specific alloys [34,35], while others have provided a brief overview of the processes of wear generation and corrosion [36–38]. However, there is a need for more comprehensive studies that investigate the effects of different factors such as the manufacturing process, surface finish, and environmental conditions on the corrosion and wear behavior of additively manufactured metal parts in biomedical applications. Additionally, some studies have only focused on the corrosion or wear behavior of the materials, but not both [39]. Therefore, a more holistic approach that considers both corrosion and wear behavior is necessary. Overall, the study of corrosion and wear behavior of additively manufactured metal parts in biomedical applications is an important area of research that requires further investigation to ensure the safety and reliability of biomedical implants. This study aims to investigate the corrosion and wear behavior of additively manufactured metal parts in the context of biomedical applications. Specifically, the research seeks to understand the mechanisms of corrosion and wear in additively manufactured alloys, the influence of processing conditions on microstructure and subsequent corrosion and wear resistance, and the anisotropic behavior of corrosion and wear due to the layered structure of additively manufactured alloys.

2. Factors That Influence Corrosion Performance and Wear Performance of AM-Manufactured Biometals

2.1. Factors That Influence Corrosion Performance

The number of 3D printable metals is limited, including stainless steel, AlSi10Mg, Fe-based, Ti-based, Co-based, Mg-based, and Ni-based alloys [40,41]. Moreover, high cooling rates lead to some issues that may finally influence the wear and corrosion response via the production of preferential corrosion zones, such as the generation of nonequilibrium phases and compositions due to extreme cooling rates [42–44], creation of molten pool boundaries [45], and the presence of cracks, pores, and rough surfaces [46–48]. For instance, it was proved that the presence of pores in the additive manufactured (AM) parts decreases the passivity of the material [49]. The porosity issue, whether as the trapped gas kind or from unmelted powders, can be prevented by the optimization of AM and 3D printing conditions (reduction in scanning rate, increasing the laser power) [50,51]. In addition to printing conditions, surface engineering and post-processing can remove pores [52]. The existence of pores may lead to the local acidification and depassivation of the material from inside of the pores, which is expedited by cathodic activity from outside of pores [53]. Meanwhile, the size, geometry, and distribution of the pores also play a role in the overall corrosion performance.

It was reported that molten pool boundaries (MPBs) are a common issue of SLMed parts, which can cause thermal stress, elemental segregation, and generation of non-equilibrium phases, finally inducing localized corrosion [45]. Moreover, the other issue regarding the SLM method is the roughness due to the Marangoni force, improper powder melting, the balling phenomenon, irregular and unstable melt pool, and evaporation during the powder melting [54,55]. Broadly speaking, surface characteristics have a great impact on the corrosion properties of materials due to their direct intervention in interfacial reactions with the surrounding environment, pitting susceptibility, and finally corrosion rate [56,57]. Numerous reports are showing that an increment in the roughness can lead to an increase in cracking initiation, oxidation kinetics, corrosion rate, and pitting susceptibility in stainless steel, copper, magnesium, etc. [58–64]. It should be noted that surface treatment and the improvement of roughness on AMed parts is a very challenging task especially for complex-shaped samples, so these should be considered before any printing process and the suitable technique and optimized processing parameters should be chosen. The difficulty of reaching an excellent surface finish in AM-produced parts comes back to powder trapping inside the mesh structure during the 3D printing process, which is very hard to remove because of the blind spots issue [65–69]. Among other problems of

printed materials, anisotropy can be mentioned, which is mainly caused by the divergent rates of solidification in various directions and heat conductivity, leading to an anisotropic corrosion response and mechanical properties [70,71]. Additionally, the varied physical structures in the different planes can lead to versatile corrosion behavior [72]. It was observed that the effect of anisotropy became more significant in harsh conditions and aggressive solutions.

Electrochemical Impedance Spectroscopy (EIS) is a technique used to measure the corrosion rate and electrochemical behavior of materials, such as Ti and Mg alloys. EIS can provide reliable and repeatable estimations of the instantaneous corrosion rate [73]. Some studies have used EIS to investigate the corrosion behavior of various alloys manufactured using different AM methods, such as laser powder bed fusion, direct energy deposition, wire arc additive manufacturing, and binder jetting. In this regard, the similarities and differences between the equivalent electrical circuits (EECs) obtained from EIS results for alloys manufactured using different AM methods have been studied. A comparative EIS study of the native oxide layer of selective laser-melted and wrought alloys has been conducted, analyzing the EECs of these materials [74]. The electrochemical response linked to the native oxide layer of the AM-manufactured materials was found to be best fitted by the Young impedance model, which assumes that resistivity through the oxide layer varies exponentially. In comparison to the SLM specimen, the wrought 316L stainless steel sample's passive layer capacitance was consistently higher (about 1.8 times higher). Consequently, the oxide layer dielectric constant of the wrought material was greater (~1.8 times higher) than the oxide film dielectric constant of the SLM 316L sample due to the roughly constant oxide film thickness across all samples [74]. Furthermore, EECs have been used for the impedance spectra analysis of various materials and plasma electrolytic oxidation (PEO) coatings [75]. These studies provide insights into the unique EECs associated with different AM methods and their respective materials.

Furthermore, the influence of process parameters on EECs for a stated AM method can be significant. Factors such as the composition of the alloy, microstructure, and the presence of protective coatings can impact the EECs obtained from EIS results. Additionally, machine learning models have been employed to predict the impedance data of EIS, offering a potential avenue to understand the influence of process parameters on EECs for a given AM method [76]. The influence of process parameters on EECs for a stated AM method is a complex area of study, with factors such as alloy composition, microstructure, and protective coatings playing significant roles in shaping the EECs obtained from EIS results.

Anti-Corrosion Bioactive Coatings

Bioactive coatings with anti-corrosive properties are being developed for a variety of applications, including metallic bone implants. These coatings aim to improve the corrosion resistance of the implants and prevent implant failure. Several techniques and materials are being explored for this purpose, such as sol-gel coatings, nanocomposites, and hybrid coatings. For instance, a study discusses the use of a polymerized 3-aminopropyltriethoxysilane (APTES) layer and PLGA mixed with SDS to create a bioactive coating with antibacterial and anticorrosive properties on a specific alloy bone implant [77]. Another study highlights the effectiveness of hybrid anticorrosive bioactive PEO coatings for biomedical products made from Mg and its alloys, assessing their corrosion-protection level using various methods [78]. Additionally, nanocomposite coatings are being developed with enhanced corrosion and wear resistance, as well as superior mechanical and tribological properties [79]. These advancements in multifunctional bioactive coatings hold promise for improving the performance and longevity of metallic implants, including bone implants.

A protective coating for Mg alloys can improve their corrosion resistance [80,81], and additive manufacturing techniques, such as laser powder bed fusion (LPBF), have been explored for this purpose [82,83]. One study developed a magnesium–aluminum alloy (Mg-10.6Al-0.6Zn-0.3Mn) with a record low degradation rate among all magnesium alloys, even withstanding seawater corrosion [82]. The alloy showed enhanced passivation with

longer immersion periods. In addition to alloy development, different coating designs have been explored to improve the degradation rate of magnesium alloys. The coating is an effective way to enhance the degradation rate of MG alloys, as different coating designs can form a protective film on the surface of the Mg alloy [84]. Various types of bioactive coatings can be applied to Mg alloys via AM methods to improve their corrosion resistance. These coatings can be categorized into conversion coatings and deposited coatings. One study coated a mesoporous bioactive glass on biodegradable magnesium to improve its corrosion resistance [85]. Another study proposed a bioactive coating system to slow down the corrosion rate of magnesium alloys and accelerate the bone fracture healing process. The coating system can be applied via conversion coatings or deposited coatings [86].

Furthermore, bioactive coatings can be deposited on Ti and its alloys using AM methods to improve their corrosion resistance. One study found that the application of a bioactive coating on a Ti alloy improved its corrosion resistance [87]. Another study evaluated the effect of a biomimetic coating on a Ti substrate, which showed improved bioactivity and corrosion resistance [88]. Additionally, recent research has focused on developing novel smart coating systems that facilitate better corrosion protection and longer service life [89].

2.2. Factors That Influence Wear Performance

Wear is the destruction/removal of material per unit of time happening due to friction with another component via mechanical procedures such as relative movements between two various components. Different factors such as material characteristics and mechanical properties are able to reduce the wear value [90]. Wear occurs through some well-known mechanisms, including adhesion wear, abrasion wear, erosion, fatigue, fretting, and oxidative wear with the two different intensities of mild wear (~0.01–1 mm in debris particle size) and severe wear (larger wear debris sizes ~20–200 mm) [91]. In addition, wear occurs in three stages: the first stage has an unstable wear rate, while the middle stage usually has a steady low wear rate, and the final stage exhibits a faster wear rate.

Wear resistance refers to a material's ability to resist material loss due to mechanical action such as abrasion, edge cutting, impact, and repeated rubbing or scraping. It is an important property for materials used in applications involving contact. Wear-resistant materials minimize friction between mating surfaces, allowing parts to retain their form and integrity for longer. The key factors influencing wear are temperature, sliding speed, hardness, modulus of elasticity, load, and composition of material. The wear mechanisms include abrasive wear, adhesive wear, erosion wear, and cavitation erosion. The wear process can change continuously in time or with changes in operational conditions. The wear rate, also known as the K factor, is a measure of a material's resistance to wear [92].

It should be noted that the wear rate depends upon the shape and geometry, the kind of materials, hardness, and toughness of the surface, presence of abrasive resistant phases and particles in the material, AM processing parameters (scanning speed, energy), post-processing by heat treatments, working state, and the formation of tribofilms [93]. Generally, AM-manufactured metals exhibit an equal or higher wear resistance compared to traditional composite materials. It was reported that the utilization of a 3D-printed composite material with high filler content can considerably improve wear resistance, so it was recommended for long-term uses [94]. In addition, it was proved that the right material selection can impact two-body wear behavior [95]. The aging and processing condition of the 3D-printed material was also shown to be an influential factor in the wear response [96].

3. Titanium and Its Alloys

Titanium alloys are among the best choices for applications in the biomedical industry due to their numerous advantages, such as favorable biocompatibility, bioactivity, osseointegration, vascularization, low elastic modulus, high specific strength, etc. [97]. Moreover, Ti alloys exhibit high corrosion performance despite the complex and harsh condition of physiological body fluids containing attacking ions, such as Cl^- , Na^+ , Cu^{2+} , and K^+ , and

sulfates, bicarbonates, phosphates, lymph, plasma, glucose, and proteins [98]. Thus, Ti alloys are used for biomedical applications such as orthopedic implants [99], dental implants [100], cardiovascular devices [101], surgical instruments [102], spinal implants [103], load-bearing biomedical devices, and implants [104]. It should be noted that despite the excellent corrosion performance of Ti, there are several dangers, including tribocorrosion, local corrosion, and ion precipitation in the body environment, and these lead to concerns about the long-term utilization of Ti alloys, adversely altering surface properties and corrosion performance of the Ti alloys. This issue cannot be ignored and neglected since the corrosion of implant material may result in implant failure, reducing the lifetime of implants, and serious physical harm as corrosion products enter the peripheral tissues and surround the Ti implants [26].

Recently, modern Ti implants have been produced through SLM and EBM additive manufacturing techniques and attracted much attention; however, the corrosion and wear of these modern AM-produced Ti-based materials need to be thoroughly investigated. A new class of these implants has been designed with porous structures because of their exceptional mechanical properties, bioactivity, and biocompatibility specifically using the $\alpha + \beta$ Ti-6Al-4V alloy [105,106]. One of the significant features of these porous structures is related to their high surface area leading to lower corrosion resistance. In addition, the lower electrolyte flow arising from the special geometry of pores and their connectivity can be regarded as another reason for the reduction in the corrosion resistance [107]. Contrary to this claim, other studies have shown that 3D-printed porous structures have comparable or even superior corrosion resistance [108,109]. Additionally, some researchers claim that the corrosion response of AM-produced materials resembles crevice corrosion, considering every pore as a crevice in which oxygen deficiency occurred, leading to the generation of an oxygen concentration difference cell. Therefore, due to the autocatalytic effect, the dissolution rate inside the pores is increased, and the passive films surrounding the interior of the pores deteriorate, leading to the occurrence of localized corrosion in the porous titanium alloys [110].

The electrochemical response of AM-produced porous Ti was investigated by Morris et al. [111]. They claimed that porosity can positively affect biocompatibility and osseointegration. They reported that increasing porosity levels led to reduced mechanical strength and increased corrosion characteristics. They indicated that the electrochemical response of porous AM-produced Ti samples experienced crevice corrosion and intergranular corrosion mechanisms. They also concluded that the AM-manufactured Ti samples with larger porosity showed increased corrosion values; the optimum range of porosity was revealed to be between 40% and 60% [111]. In another study, Sharp et al. [112] investigated the corrosion performance of AM-produced Ti6Al4V gyroid lattices with varied porosity values (60–80%). It was shown that the structure with 60% gyroid was susceptible to pitting corrosion in comparison to 80% gyroid and solid samples, mainly due to a higher lattice surface area to void volume ratio. However, regardless of the earlier onset of pitting corrosion, both gyroid samples had lower corrosion rates, confirming their less severe corrosion state. Figure 4a indicates the corrosion rates of solid 60% and 80% gyroid samples calculated through Tafel plots, manifesting the lower corrosion rate and corrosion severity of porous samples compared to solid samples. Additionally, Figure 4b exhibits that all samples underwent corrosion with high variability in the corrosion extent with the appearance of corrosion byproducts. It can also be observed that corrosion attacks mainly initiate and focus on special locations such as corners and raised edges. The solid sample manifested a very interconnected form, while the porous samples had distinct and isolated patches [112].

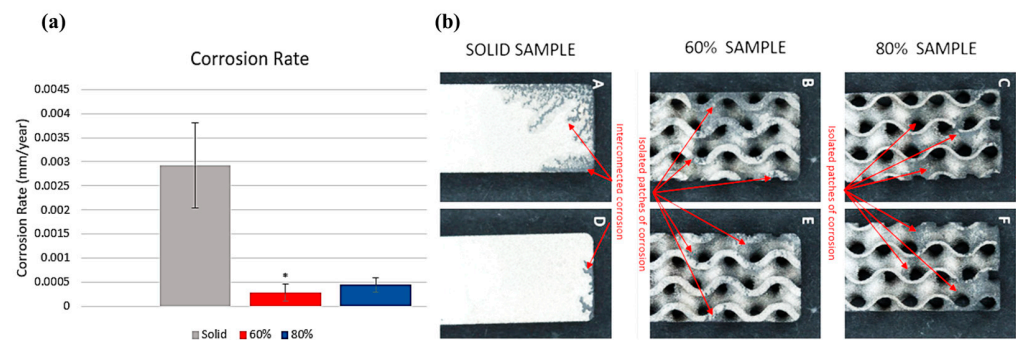


Figure 4. (a) The corrosion rate of solid and porous Ti-6Al-4V alloy, as calculated from the Tafel plots, and (b) the corrosion coverage state of two faces of solid, nonporous, and porous gyroid specimens. * Indicates 60% samples having statistical significance to solid samples ($p < 0.05$) whilst 80% porous samples having $p = 0.0532$. Adapted from [112].

For the case of bulk 3D printed Ti samples, the corrosion behavior is mainly determined through its microstructure; for instance, the SLM's higher cooling rates facilitate the fabrication of the acicular α' martensite and hinder the production of β phases that finally affect corrosion resistance. Meanwhile, during the EBM procedure and due to the preheating process before melt scanning, the cooling rate is low because of the reduced thermal gradients. Accordingly, the microstructure of the EBM-processed Ti alloys consists of coarser α lamellae with narrow β interphase regions, hence the EBM-fabricated Ti-6Al-4V sample that exhibited numerous finer lamellar α/β phases compared to wrought Ti-6Al-4V [113]. It is known that β phases improve the resistance of charge transfer and decrease the metal dissolution rate. In addition, the finer lamellar α/β structures hinder the inconsistent distribution of alloying elements, decreasing the galvanic potential between the α and β phases, leading to the superior corrosion resistance of the EBM-produced Ti-6Al-4V sample in comparison to the wrought sample [114]. The corrosion response of SLM-produced β , α , and $\alpha + \beta$ titanium alloys was investigated by Zhou et al. [115]. They indicated that the Ti-13Nb-13Zr alloy with β phase and α' acicular martensitic structure had the highest corrosion potential and the highest corrosion resistance compared to the CP Ti and Ti-6Al-4V alloy, mainly due to the existence of stable Nb_2O_5 phases that maintain the integrity of the passive oxide film. In this regard, Figure 5 shows the electrochemical Tafel curves of the samples in Ringer's solution. It can be seen that the Ti-6Al-4V sample has the least corrosion current density, while Ti-13Nb-13Zr manifests the highest corrosion potential. Therefore, the occurrence of passivation is very difficult for the SLMed Ti-13Nb-13Zr sample but whenever the passivation has occurred, the generated film is the most integrated and stable compared to the SLMed CP Ti and Ti-6Al-4V samples [115]. It was revealed that the presence of Zr and Nb elements in the Ti matrix can substantially promote the resistance toward localized corrosion due to the fabrication of ZrO_2 and Nb_2O_5 phases in passive TiO_2 layers, leading to the reduction in the Cl^- ingress and increment of the oxide film integrity [116].

Another study Pede et al. [117] investigated the corrosion response of SLM-produced β -type Ti alloys (Ti-42Nb and Ti-20Nb-6Ta) and compared them with CP Ti and Ti-6Al-4V alloys. They observed that CP Ti and Ti-6Al-4V samples only had a martensitic α' phase, while Ti-42Nb had β phase, and Ti-20Nb-6Ta consisted of orthorhombic martensitic α'' phase. The electrochemical evaluations proved that both β -type Ti alloys exhibited superior corrosion resistance, especially the Ti-42Nb alloy. Moreover, it was confirmed by the mass spectrometry that there is not any considerable release of Nb or Ta in the electrolytes, while there was clear evidence of V and Al release as a result of corrosion [117]. Additionally, β -type Ti alloys did not show any pitting corrosion or disruption of the passive film that was related to the fabrication of tantalum/niobium oxides leading to a more stable and sturdier passive layer even under very high electrical potentials. The high-temperature corrosion performance of AM-manufactured and cold-rolled Ti-6Al-4V alloy was investigated by

Liang et al. [118] and it was shown that the 3D-printed sample had a considerably higher corrosion rate, mainly due to the generation of the α' phase during fast cooling of 3D-printed Ti-6Al-4V. In this regard, Figure 6 demonstrates the weight gain of these samples at 600 °C for 200 h under air (Figure 6a) and air-SO₂ (Figure 6b) environments.

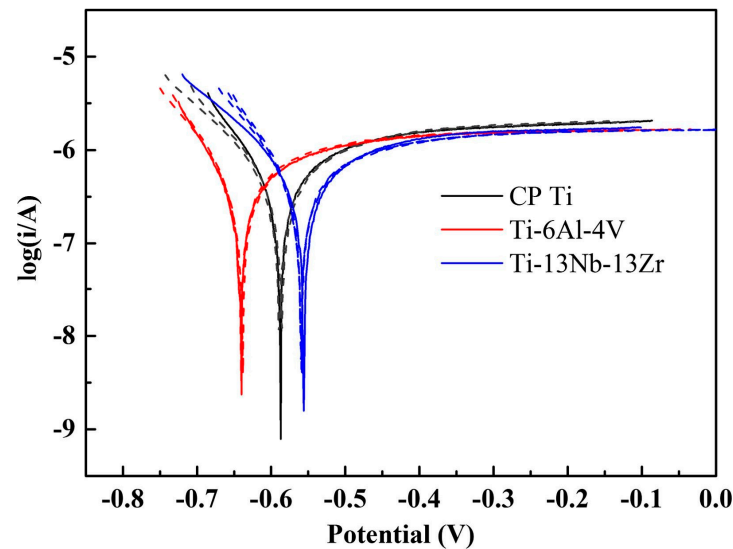


Figure 5. The polarization Tafel curves of SLM-produced Ti-13Nb-13Zr, Ti-6Al-4V, and CP Ti in Ringer's solution at room temperature. Reprinted with permission from Ref. [115]. Copyright 2019 Elsevier.

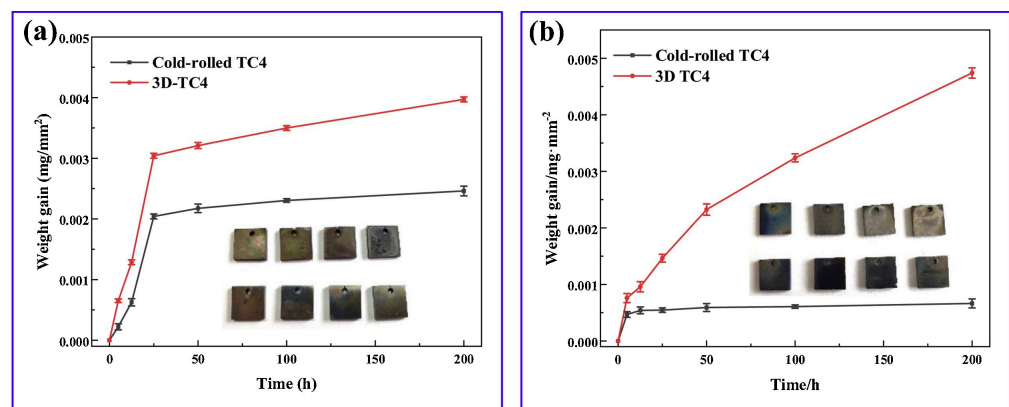


Figure 6. The plots of weight gain of 3D-printed and cold-rolled Ti-6Al-4V alloy at 600 °C for 200 h in different environments: (a) air and (b) air-SO₂. Reprinted with permission from Ref. [118]. Copyright 2020 Elsevier. Note that TC4 stands for Ti-6Al-4V alloy.

A study of the fabrication of the passive film on EBMed Ti-6Al-4V alloys was performed by Gai et al. [119] with a comparison to conventional wrought samples. It was confirmed that the passive film of the EBMed sample was thinner and more compact, which was related to finer grain sizes and a high density of grain boundaries in the EBMed sample. The grain boundaries and fine grains were recognized as active sites that are able to enhance the growth rate of the passive film based on the 3D progressive nucleation mechanism, finally leading to the improved corrosion resistance of the EBM-processed sample, schematically shown in Figure 7. As it is seen in Figure 7a, the microstructure of the EBMed sample is composed of fine α lamellar phases produced due to a fast solidification process along with prior β grains, while these α and β grains are coarse in the wrought sample as shown in Figure 7e. In addition, the related mechanism for the growth of passive film on EBMed and wrought samples is schematically presented in Figure 7b,f; during the first stage, the surface of the metal is completely covered by a continuous layer mainly

consisting of the ideal oxides TiO_2 and Al_2O_3 on the EBMed sample, while in this stage the surface of the wrought sample has a discontinuous oxide film. Because the fabrication of a passive film is a diffusion-controlled process (maintaining abridged ion diffusion channels) [120], the passive film was produced at a fast rate on the EBMed surface due to its finer grain sizes and a high fraction of grain boundaries. In this regard, the diffusion processes of preferential Ti, Al, and O occur at the grain boundaries, leading to the improvement of the oxidation process and increment of active sites for the growth of the oxide layer. Therefore, the content of TiO_2 was significantly higher in the passive film of the EBMed sample [119]. It was reported that the high content of TiO_2 in a passive layer of Ti alloys mainly has a crystalline character, enhancing the compactness and protective property of the passive layer. The nucleation, growth, and mechanism of the passive film are of high significance since they can directly influence the corrosion and electrochemical response of the materials; they can also control the transmission speed of point defects inside the passive film. Respectively, two types of models were recommended for the nucleation and growth of the passive film on reactive metallic surfaces entitled two-dimensional (2D) and three-dimensional (3D) growth models [121–126]. These models were determined based on the current time plots measured by potentiostatic polarization experiments. The corresponding current–time plots for EBMed and wrought samples are shown in Figure 7c,d,g,h in which Figure 7c,g shows the passivation current transient plots, where it is seen that the current density greatly increases to a top value due to the initiation of the oxidation reaction, soon after it was decreased during the passive film formation. Based on the maximum current I_m and maximum time t_m values, passivation started earlier on the EBMed sample and I_m was reached fewer times. Consequently, the passivation rate is faster on the EBMed sample compared to the wrought sample [119].

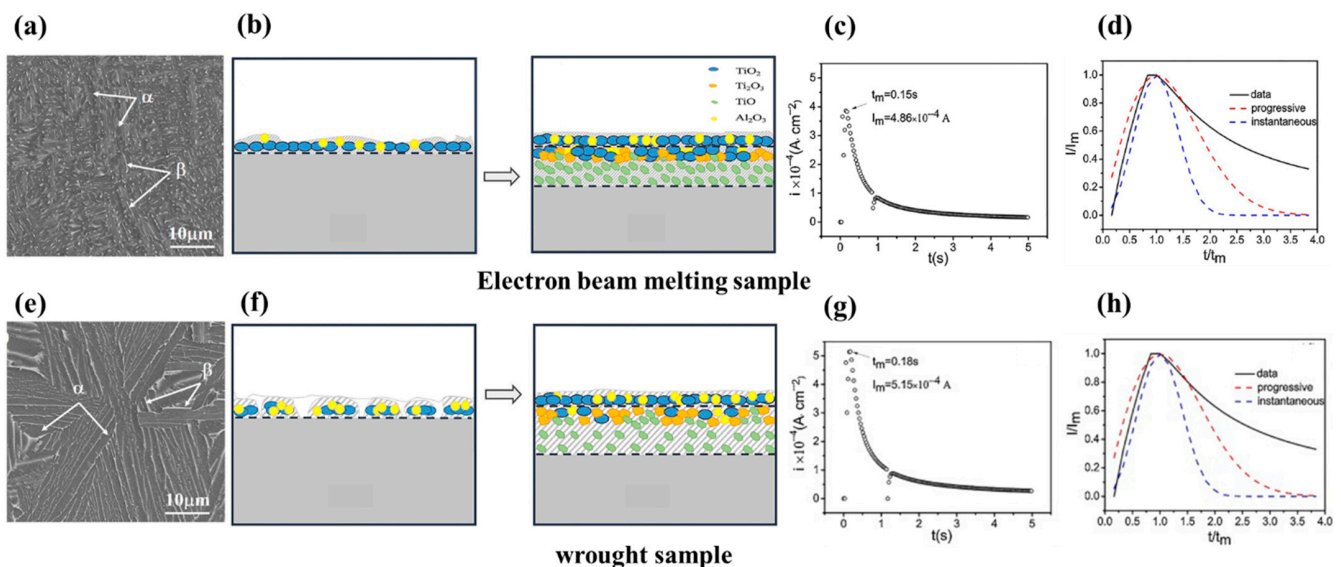


Figure 7. (a,e) The SEM micrographs of EBMed-produced and wrought Ti-6Al-4V alloys, (b,f) the passive film growth mechanisms for EBMed and wrought samples, (c,g) the current–time curves for estimation of maximum passive current (I_m) and passive time (t_m) for EBMed and wrought samples, and (d,h) the comparison plots of the current–time curves ($I/I_m - t/t_m$) with the instantaneous and progressive nucleation model lines for EBMed and wrought samples. Reprinted with permission from Ref. [119]. Copyright 2018 Elsevier.

In addition to passive film characteristics, the surface roughness, wettability, and microstructure can greatly influence the electrochemical reactions. In this regard, Casadebaigt et al. [122] studied the effect of surface roughness and microstructure on the oxidation kinetics of laser beam melting (LBM)-processed Ti-6Al-4V alloy at 500–600 °C. They also investigated the post-processing of these samples through HIP (hot isostatic pressure) treatment, rolling, and annealing. The microstructure of the LBMed sample includes α'

acicular martensite and initial β grains elongated toward the building direction. During isothermal oxidations at 500–600 °C it was deduced that the kinetics of oxidation followed a parabolic law. Moreover, it was observed that the weight gain of LBM samples was twice as much as grounded LBM samples, which was attributed to its larger specific area and the oxidation of partially melted powder; this information can also be found in Figure 8.

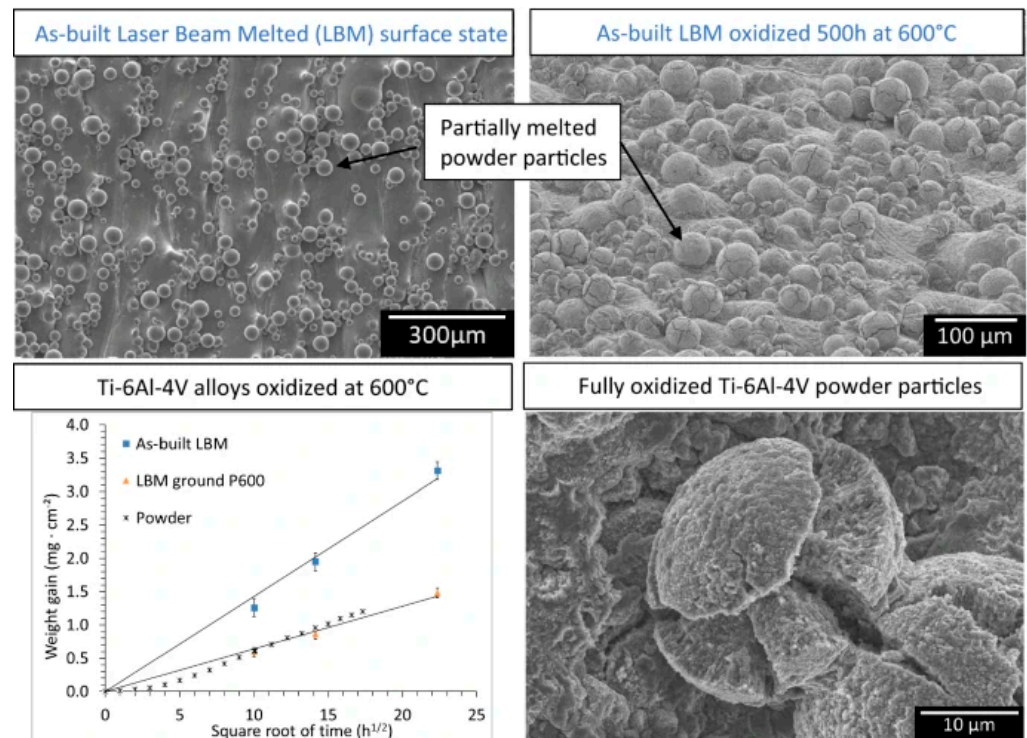


Figure 8. The microstructure and weight gain of LBM-manufactured Ti-6Al-4V specimens. Reprinted with permission from Ref. [122]. Copyright 2018 Springer.

The wear performance of AM-manufactured Ti alloys for biomedical applications has been the subject of significant research. Surface modification has emerged as a key approach to enhancing the wear resistance of Ti alloy surfaces, with additive manufacturing being a focus of attention [104]. Laser-engineered net shaping (LENS), an additive manufacturing technology, is thought to be able to directly coat alloy surfaces. Implant surfaces that are flat or curved can benefit from this line-of-sight process, which increases implant surface resistance to corrosion and wear [104]. The inherent irregularities on the surface of AM components that lead to poor wear performance are due to the solidification of the melt pool, leading to partially melted powder particles on the component surface [127], which are in the range of 10–60 μm in diameter for SLM powders and 50–150 μm for EBM powders [128]. Furthermore, the layer-by-layer deposition in AM causes surface defects such as the stair-step effect [129]. Heer et al. [130] directly coated the surface of CP Ti with silica using LENS, and during the wear test, an in situ friction film formation was seen, indicating the material's self-healing capabilities. This material not only had a good hardness of 1500 HV but also showed good electrochemical qualities without being cytotoxic. SiC powder was injected into a Ti melt pool using a high-power laser to create a SiC-reinforced Ti matrix composite (TMC) using the LENS technique. This composite coating was applied to CP Ti implants, improving Ti's resistance to corrosion and wear by approximately 100 times [131].

4. Magnesium and Its Alloys

Magnesium and its alloys are among the greatest candidates for the production of biodegradable implants due to their exceptional physical and chemical properties, such

as low density, high specific strength, favorable damping performance, biocompatibility, biodegradability, similar Young's modulus with natural bone, nontoxicity, etc. These Mg-based components and implants can be produced by the utilization of modern additive manufacturing technologies [15,132,133]. Thus, Mg alloys are used for applications such as orthopedic implants, cardiovascular stents, dental implants, surgical sutures, bone fixation devices, and drug delivery systems [134,135]. One of the most widely used classes of Mg-based alloys is the WE43 alloy (Mg-4Y-3RE-Zr), which contains rare earth elements, such as Nd, Y, Dy, Gd, and Zr, exhibiting a combination of strength, plasticity, and enhanced corrosion performance [136]. Lovašiová et al. [137] investigated the electrochemical response of SLM-produced WE43 magnesium alloy in simulated body fluid (SBF) and reported that the 3D-printed alloy had more positive corrosion potential values compared to the as-cast alloy. This superior corrosion behavior is due to the existence of oxides with a nobler nature in the SLM-produced alloy. It was also shown that the microstructure can greatly affect the corrosion rate of material in the SBF solution. Furthermore, the presence of porosities and yttrium oxide inclusions can generate active paths for the corrosion attack, which facilitates the penetration of the corrosive agents. Figure 9 shows the corrosion products on the surface of the 3D-printed alloy that mainly include mixed calcium–magnesium phosphates and carbonates with P, O, Mg, and Ca elements.

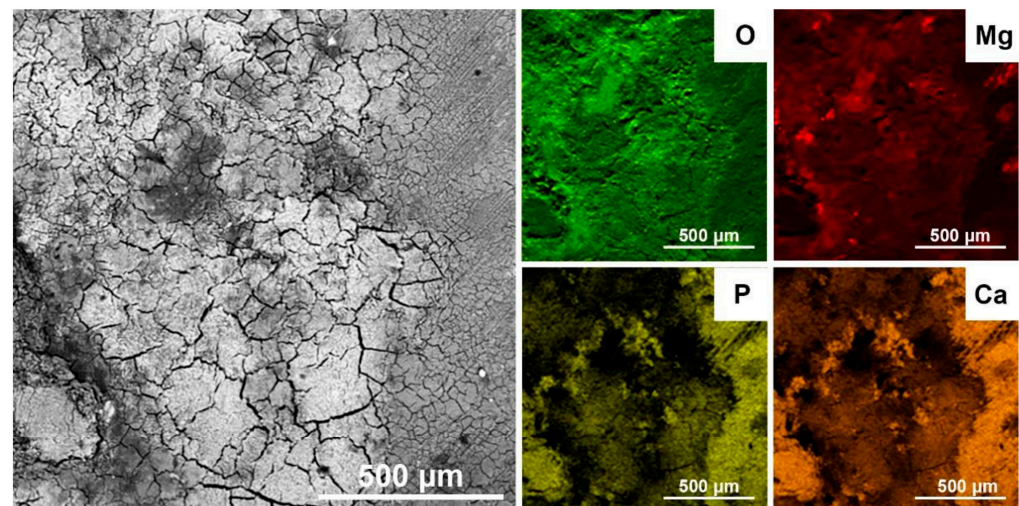


Figure 9. The corrosion products on the surface of the 3D-printed WE43 alloy along with element distribution maps (EDS); reprinted from [137].

In another study, Dong et al. [138] studied the corrosion performance of the 3D-printed biodegradable Mg scaffolds with porous structures that could be utilized for bone defects as temporary bone substitutes. They used an extrusion-based AM method and a special process to design the porous structures with highly interconnected structures along with using MgF_2 -CaP and MgF_2 coatings to promote corrosion resistance and biocompatibility; this procedure is shown in Figure 10. It was proved that these coatings are not only able to fully cover the struts but also, they can infiltrate the struts by micropores, leading to a reduction in macro- and micro-porosity. Because of the highly interconnected porous structure of the bare sample, it had low corrosion resistance while the MgF_2 -CaP coatings considerably promoted the corrosion resistance and reduced the biodegradation rate. Generally, it was proved that porosity can directly affect corrosion performance and cell behavior.

In another study, Li et al. [139] utilized an SLM device to produce a topologically ordered porous WE43 scaffold with the diamond unit cell structure and investigated the in vitro biodegradation behavior. They observed an uncommon biodegradation mechanism in these samples starting with uniform corrosion that was followed by localized corrosion (specifically in the scaffolds' center region). They proved that this ordered topological de-

sign can be a great option for the design of multifunctional bone substituting implants with adjustable biodegradation profiles. The increment in the immersion time in these samples led to the production of white degradation products on the struts' surface (Figure 11a), but samples even after 28 days still maintained their structural integrity without considerable detachment of degraded particles. In the early times, hydrogen gas evolution rapidly increased, then it gradually slowed down, but after 4–6 days the slope of the hydrogen release increased again as shown in Figure 11b. In addition, the Mg ion concentration increased, while the concentrations of P and Ca ions decreased (Figure 11c). The pH changes have different manners according to location as shown in Figure 11d,e. The electrochemical measurements by Tafel plots confirmed the occurrence of a passivation stage in the anodic polarization branches in all samples (Figure 11f). According to Figure 11g, the corrosion current density increased from 3×10^{-5} to 6×10^{-5} $\text{A}\cdot\text{cm}^{-2}$ during the first 24 h, then it fell after 24 h, finally reducing to 2×10^{-5} $\text{A}\cdot\text{cm}^{-2}$ by day 14. The scanning electron micrographs confirmed these results as presented in Figure 12a,b, indicating that WE43 (white) was replaced by degradation products of a gray color mainly concentrated at the center of the scaffolds rather than at the periphery. In this regard, Figure 12c schematically represents the suggested degradation mechanism. The biodegradation rate was estimated to be about $\approx 20\%$ volume after 4 weeks.

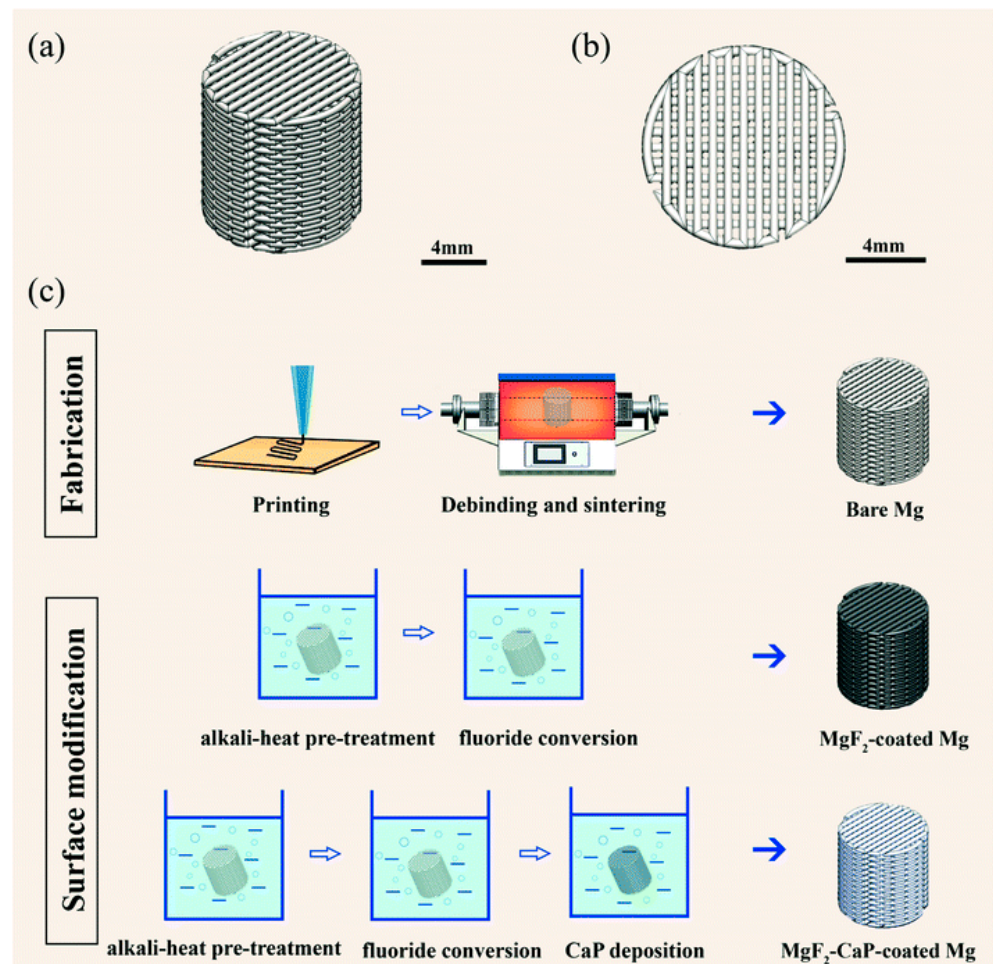


Figure 10. A schematic presentation of the steps in the additive manufacturing of porous Mg scaffolds with highly interconnected structures: (a,b) porous magnesium scaffold design and (c) schematic images of the scaffold fabrication and surface modification. Reprinted with permission from Ref. [138]. Copyright 2021 Royal Society of Chemistry.

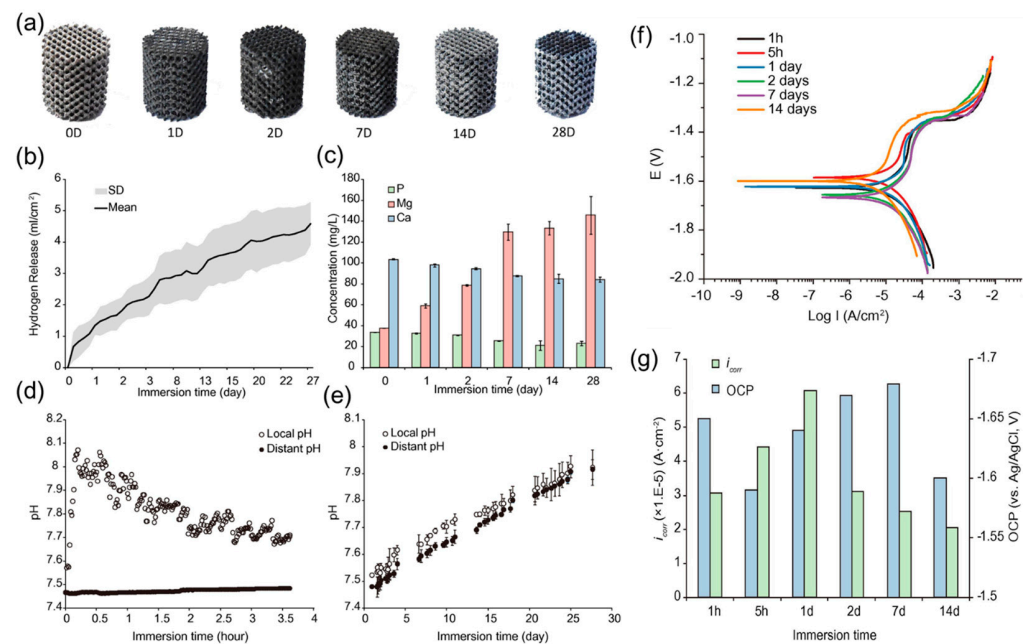


Figure 11. Results of in vitro degradation and corrosion tests on Mg specimens: (a) as-degraded specimens, (b) hydrogen release, (c) P, Mg, and Ca release, (d,e) pH variation in short-term and long-term conditions, (f) potentiodynamic polarization curves, and (g) variation of open circuit potential (OCP) and corrosion current density (i_{corr}) with specimen immersion. Reprinted with permission from Ref. [139]. Copyright 2018 Elsevier.

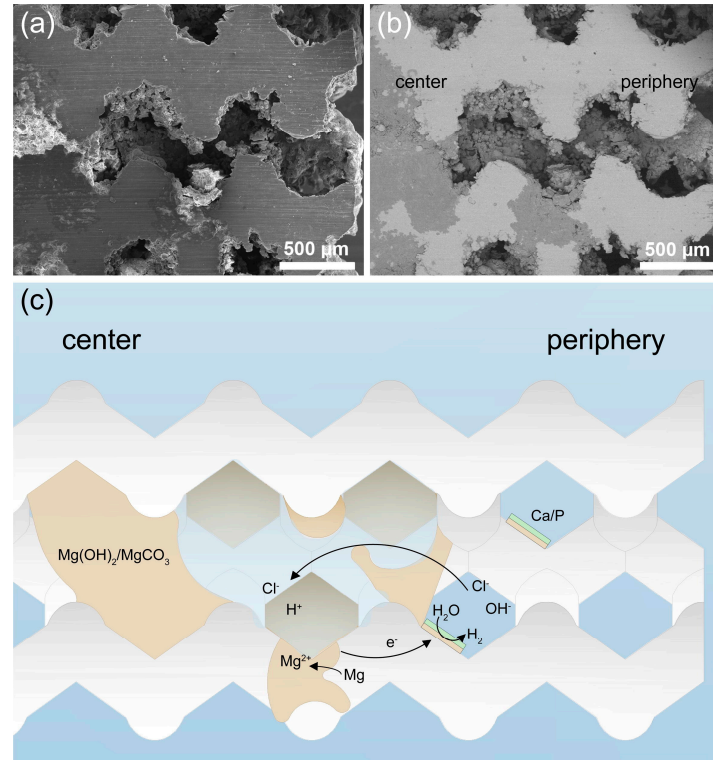


Figure 12. Micrographs of degraded Mg scaffolds after 7 days of immersion: (a) scanning electron micrograph, (b) back-scattered electron micrograph, and (c) schematic presentation of the proposed degradation mechanism at the center of the WE43 scaffolds; adapted with permission from Ref. [139]. Copyright 2018 Elsevier.

A protective coating for magnesium alloys can improve their corrosion resistance [80,81], and additive manufacturing techniques, such as laser powder bed fusion (LPBF), have been explored for this purpose [82,83]. One study developed a magnesium–aluminum alloy (Mg-10.6Al-0.6Zn-0.3Mn) with a record low degradation rate among all magnesium alloys, even withstanding seawater corrosion [82]. The alloy showed enhanced passivation with longer immersion periods. In addition to alloy development, different coating designs have been explored to improve the degradation rate of magnesium alloys. The coating is an effective way to enhance the degradation rate of MG alloys, as different coating designs can form a protective film on the surface of the Mg alloy [84]. Various types of bioactive coatings can be applied to Mg alloys via AM methods to improve their corrosion resistance. These coatings can be categorized into conversion coatings and deposited coatings. One study coated a mesoporous bioactive glass on biodegradable magnesium to improve its corrosion resistance [85]. Another study proposed a bioactive coating system to slow down the corrosion rate of magnesium alloys and accelerate the bone fracture healing process. The coating system can be applied via conversion coatings or deposited coatings [86].

The wear performance of AM-manufactured Mg alloys for biomedical applications is a critical aspect of their suitability for use in medical implants but unfortunately, it is rarely studied. Research has shown that the wear performance of Mg alloys can be enhanced through the use of specific alloying elements and design strategies. For example, the addition of Al and Si has been found to improve the wear resistance of Mg alloys [34]. It is known that the wear resistance of AM-manufactured Mg materials can be influenced by factors such as material composition, porosity, and post-processing treatments. It is important to consider the impact of the deposition angle, heat treatment, and printing temperature on the mechanical properties and wear behavior of 3D-printed metal alloys, including Mg-based alloys. Additionally, the presence of other elements such as zinc in Mg alloys can influence their mechanical characteristics and degradation rate [140,141].

5. Ferrous Alloys

Stainless steel (SS) as an Fe-based alloy is regarded as one of the most well-known biomaterials. It contains a Cr element that has high corrosion resistance. The most popular stainless steel is 316L with the composition of 16–18.5% Cr, 10–14% Ni, 2–3% Mo, <2% Mn, <1% Si, <0.045% P, <0.03% S <0.03% C, and balance Fe; this alloy can be successfully used in biomedical implants, including artificial eardrums, cardiovascular implants, orthodontic applications, and bone fixation devices [142]. By considering the above applications, the utilization of AM methods to manufacture SS implants and biomedical devices is highly favorable. In this regard, many investigations were focused on studying the corrosion performance of additively manufactured stainless steels [143]. It was deduced that 3D printing conditions such as any variation in laser power, scan speed, and the energy density of the laser can influence the microstructure, grain size, and sample voids that considerably affect the corrosion performance. It was also reported that the post-treatment influences the passive film stability and its properties, its repassivation potential, and the composition of oxide in AM-produced 316L SS. Moreover, heat treatment processes were considered one of the most influential factors in the corrosion behavior of AM parts, including the solution treatment, the heat treatment, and the aging treatment, which may have a significant impact on corrosion resistance. Finally, it was concluded that the microstructure and the grain size, the passive film, its porosity, surface roughness, and its other characteristics, the Cr distribution, and the embedded parts can affect the corrosion response of the Fe-based AM parts. In one study, Wang et al. [144] studied the tribocorrosion response of additively manufactured 316 stainless steel, and they utilized a bronze-infiltrated binder jet to conduct 3D printing and then evaluate the corrosion response of the produced composite in the seawater environment. They reported a significant improvement in the wear behavior of this material due to the fabrication of a passive oxide film acting as a tribofilm, preventing abrasive wear in conditions of high loading. The results of wear tests including wear rates and average friction coefficients are shown in Figure 13. Unfortunately, they reported

a lower corrosion resistance in AM composites compared to the traditional 316 SS alloy in seawater, exhibiting a higher anodic activity. Figure 14 presents a schematic of the suggested tribocorrosion mechanism, indicating that lower loads lead to a lower friction coefficient due to the smeared soft Cu with a lower strength of shearing that maintains the required lubrication. The increment in pressure during sliding can induce the abrasive wear and facilitate the corrosion process, then the produced passive film due to corrosion plays a lubricating film role that subsequently minimizes the abrasive wear [144].

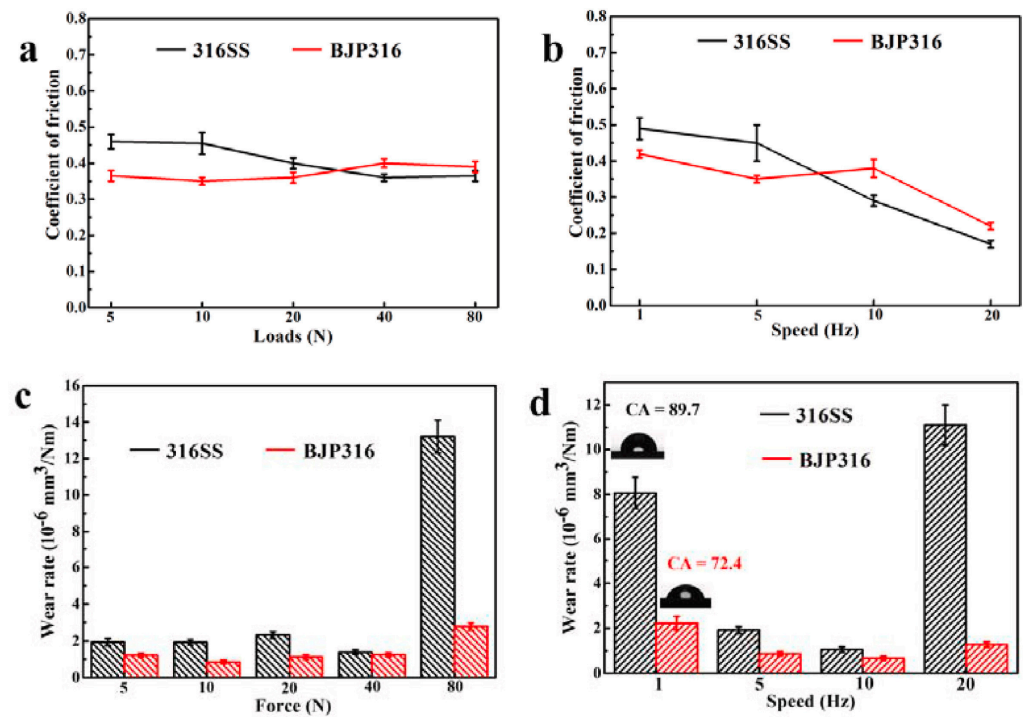


Figure 13. Wear performance of AM 316SS/bronze composite: (a,b) friction coefficients and (c,d) specific wear rates of the samples as a function of applied loads at a constant speed of 5 Hz and speeds at a constant load of 10 N. Reprinted with permission from Ref. [144]. Copyright 2020 Elsevier.

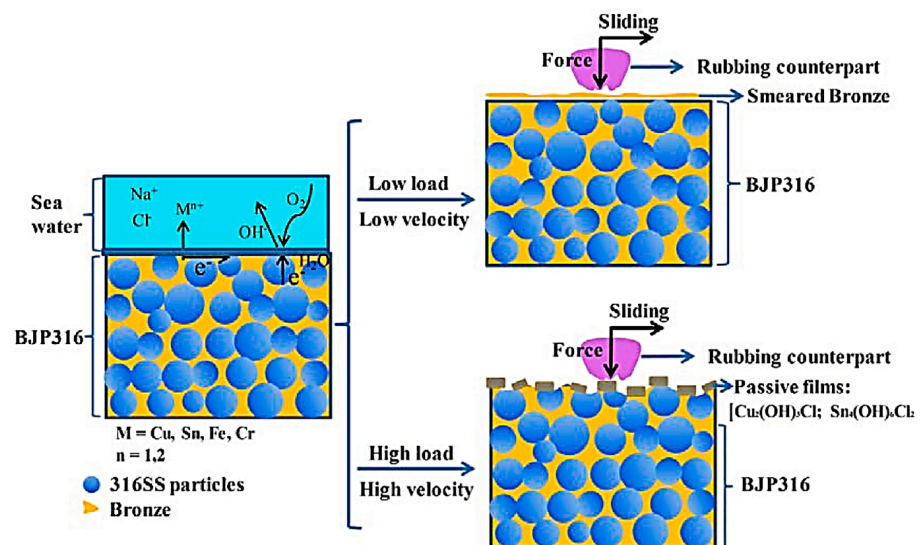


Figure 14. A schematic presentation of the proposed tribocorrosion mechanism of BJP-manufactured 316SS/bronze composite. Reprinted with permission from Ref. [144]. Copyright 2020 Elsevier.

In another investigation, Candela et al. [145] analyzed the wear response of the highly reinforced 316L/SiC_p that was manufactured by the laser-directed energy deposition (DED) method. They studied the effect of SiC particles (SiC_p) addition to 316 SS of different magnitudes. They concluded that an increment in the SiC_p content promotes wear performance (the reduction in composite mass loss). It was shown that a composite with 40 wt.% SiC_p has five-fold hardness and ten-fold wear resistance compared to bare 316L, while an increment in the SiC_p content up to 60 wt.% led to a lower friction coefficient due to the generation of the graphite. Finally, they reported that the SiC_p addition significantly transformed the wear mechanisms, changing it from adhesive type for unreinforced 316L to delamination, abrasive, and oxidative types for reinforced composites as illustrated by details in Figure 15 [145]. In another study, Tonolini et al. [146] reported the trio-corrosion behavior of 18Ni-300 maraging steel, which was fabricated by a laser-based powder bed fusion method. Their results showed insignificant variations in the wear rate between forged and AM samples (less than 5%), while there were significant differences in the microstructure of these two types of samples. While the microstructure of the forged sample is made up of blocks of lath-type martensite, the AM parts' microstructure is a fully dense fine cellular martensitic structure with the boundaries of the melt pools and scan tracks clearly visible even after the aging treatment. In addition, AM samples indicated slightly better corrosion resistance (I_{corr} : $\sim 1 \mu\text{A}/\text{cm}^2$) compared to forged ones (I_{corr} : $\sim 2 \mu\text{A}/\text{cm}^2$) [146].

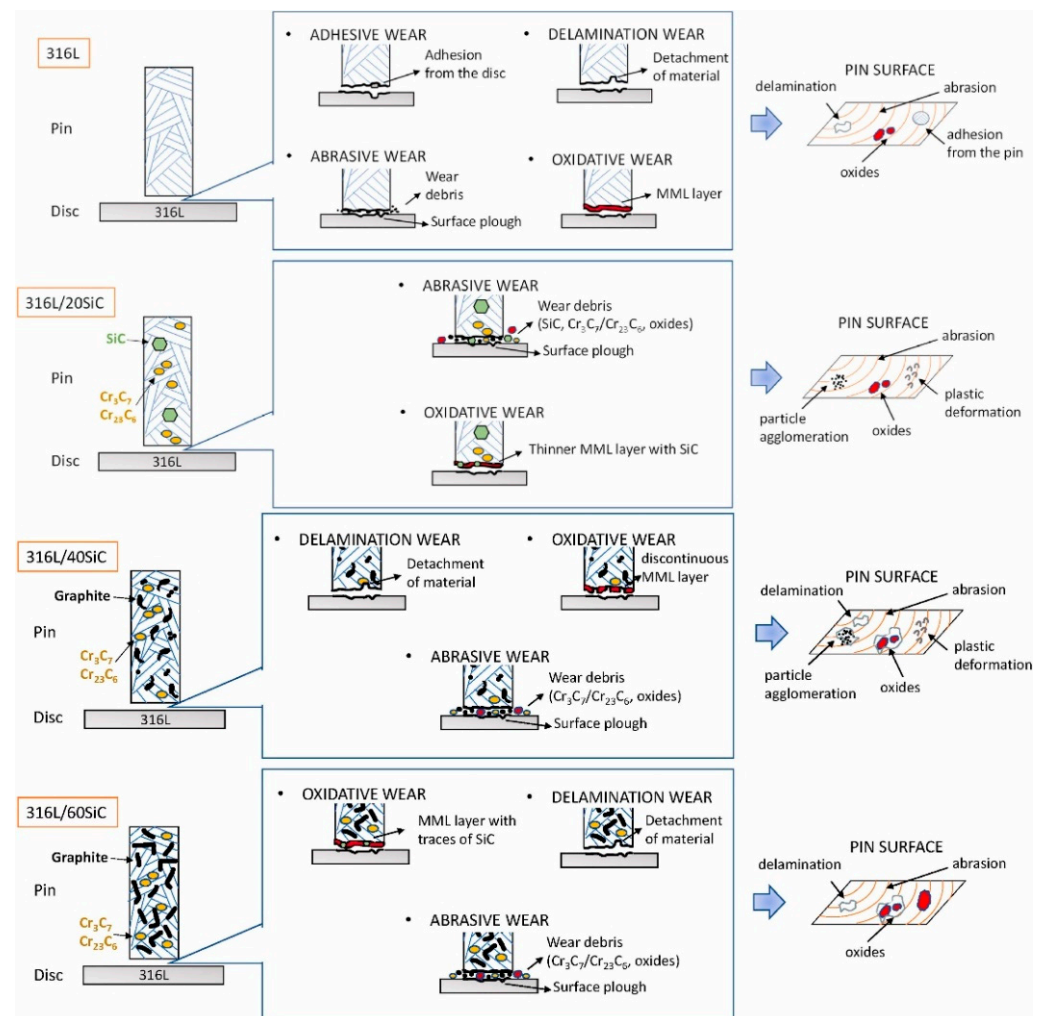


Figure 15. A schematic presentation of the proposed wear mechanisms for 316L, 316L/20SiC composite, 316L/40SiC composite, and 316L/60SiC composite. Reprinted with permission from Ref. [145]. Copyright 2022 Elsevier.

The corrosion performance of additively manufactured (AM) ferrous alloys has been the subject of significant research, with a focus on stainless steel alloys such as Type 316L. Corrosion studies of AM-prepared Fe alloys have primarily been reported for Type 316L, but a smaller number of studies have also investigated other steels. Environments containing chloride ions are known to be detrimental to the durability of various alloys, with some studies focusing on such electrolytes. The corrosion properties of AM-prepared Fe alloys have been influenced by factors such as alloy composition and the pH of the environment [147]. The large thermal gradients and rapid solidification inherent during the AM process can provide an ideal environment for the formation of Austenitic stainless steels, which can experience stress corrosion cracking (SCC) and hydrogen-induced cracking (HIC) [148]. In summary, the corrosion performance of AM ferrous alloys can be influenced by various factors, including alloy composition, environmental pH, and AM process parameters.

6. NiTi Shape Memory Alloys

Recently, shape memory alloys with near-equiatomic NiTi compositions (known as Nitinol ($\text{Ni}_{50.8}\text{Ti}_{49.2}$)) found many biomedical applications due to their exceptional in vitro/in vivo biocompatibility, superelasticity, shape memory effect, and excellent corrosion performance. These beneficial NiTi alloys as the most extensively used Ti alloy in biomedicine have the capability to be produced by 3D printing and AM technologies. Thus, these alloys are used for applications such as orthodontic wires, endodontic files, dental implants, orthopedic implants, vascular applications, neurological applications, surgical instruments, and hard-tissue replacement materials [149–152]. In one study, Buciumeanu et al. [153] investigated the synergistic effects of corrosion and wear on a NiTi alloy compared to a Ti-6Al-4V alloy. They utilized a laser-engineered net shaping (LENS) method to produce both NiTi and Ti-6Al-4V alloys. Both alloys demonstrated an improved wear resistance, while the NiTi alloy showed a lower tendency to corrode and a lesser ion release susceptibility compared to the Ti-6Al-4V alloy. In another study, Ma et al. [154] evaluated the corrosion response of an SLMed NiTi alloy after its post-processing by femtosecond laser shock peening (effect of scanning space). They reported that proper femtosecond laser treatment with optimized parameters could significantly promote the surface strength and corrosion resistance of the SLMed NiTi alloys. In this regard, Figure 16 presents the electrochemical corrosion response of the SLMed NiTi alloy in 3.5 wt.% NaCl solution during various processing parameters. It can be seen from the potentiodynamic polarization curves in Figure 16a that the I_{corr} was the lowest under the condition of 10 μm (scanning space of femtosecond laser shock peening) mainly due to the generation of TiO_2 that was protecting the substrate. In addition, the extremely large remelting area can cause the surface's overburning and the formation of cracks and holes. Moreover, the impedance measurements in Figure 16b–d reveal that the 10 μm sample has the largest Nyquist loop and the highest $|Z|$ value (low-frequency impedance modulus) along with the largest phase angles in the medium frequency range compared to the others, confirming its superior corrosion protection performance. In another study, Zhang et al. [155] investigated the electrochemical response of the EBM-processed NiTi samples by varied speed function and focus offset. These varied parameters led to different defect numbers and types, finally influencing the corrosion behavior. They concluded that high numbers of cracks led to poor corrosion resistance, while a low number of small pores with uniform distribution in the EBMed NiTi alloy led to a superior corrosion resistance nearly similar to the wrought NiTi alloy.

In addition to conducted studies about the electrochemical response of AM-manufactured NiTi alloys, some studies were focused on the wear performance of these materials. For instance, Lu et al. [156] investigated the La_2O_3 addition as a coating layer on the wear response of NiTi alloy fabricated using the direct metal deposition (DMD) AM technique. Their results indicated that the La_2O_3 coating can substantially transform and refine the microstructure of DMDed NiTi alloy, which finally affected the wear performance. They

proved that the La_2O_3 coating layer considerably improved the wear resistance due to the increment in the superelasticity and refinement of generated hard phases. Figure 17 briefly presented the achieved results of the microstructure, friction coefficients, and wear mass loss of DMD-produced NiTi alloy with and without La_2O_3 coating. It was seen that the DMDed NiTi alloy Figure 17a,b contains a NiTi_2 phase with an fcc structure (shown as A) and an austenite NiTi phase with a bcc structure (shown as B). It was also observed that the austenite NiTi has the matrix phase including lath-like NiTi_2 phases that are randomly dispersed in the matrix. For the case of DMDed NiTi samples with the addition of La_2O_3 shown in Figure 17c,d, the primary phase was austenite NiTi along with small spherical NiTi_2 phases distributed over the austenite NiTi matrix phase. Additionally, there were two other phases named and shown as C and D in Figure 17c,d in which C was an ellipsoidal precipitated phase with a cubic structure and D was a spherical precipitated phase with an orthogonal structure. It can be seen that these phases were in close relation and connection to the NiTi_2 phase. The friction coefficient results (Figure 17e) indicated different degrees of fluctuation in various time ranges, while this quality is more serious for the case of NiTi samples due to their inhomogeneous microstructure and the presence of coarse NiTi_2 secondary phases. In addition, it can be observed that the La_2O_3 addition led to an ~18% reduction in wear rate (Figure 17f) [156]. In another investigation conducted by Liu et al. [157] it was reported that NiTi samples produced by wire arc additive manufacturing (WAAM) technology had a refined microstructure, including coarse columnar grains that were gradually refined by the increment in the wall height, an equiaxed microstructure in the upper regions, and dispersion of Ni_4Ti_3 precipitates in the matrix. It was proved that in this microstructure, the dominant form of wear was plastic deformation and wear-induced work hardening that led to nucleation and the propagation of cracks, which were considerably prevented by NiTi's superelasticity. Finally, it was concluded that re-orientation of residual martensite and stress-induced martensitic transformation play a key role in NiTi's wear performance [157].

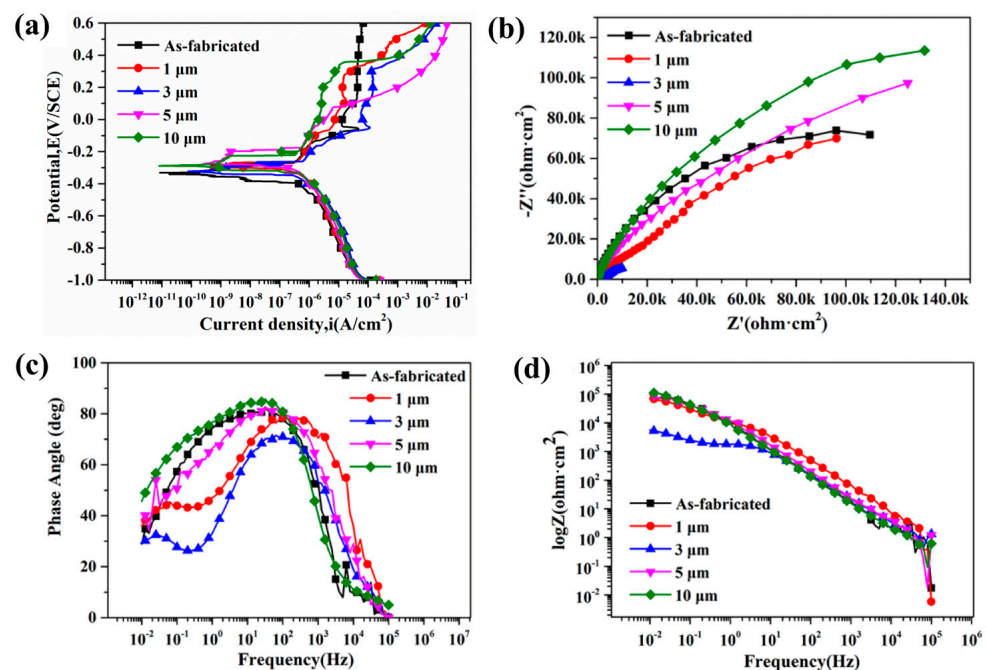


Figure 16. The electrochemical corrosion response of the SLMed NiTi alloy in 3.5 wt.% NaCl solution: (a) potentiodynamic polarization curves, (b) Nyquist curves, (c) Bode phase, and (d) Bode impedance. Adapted from [154].

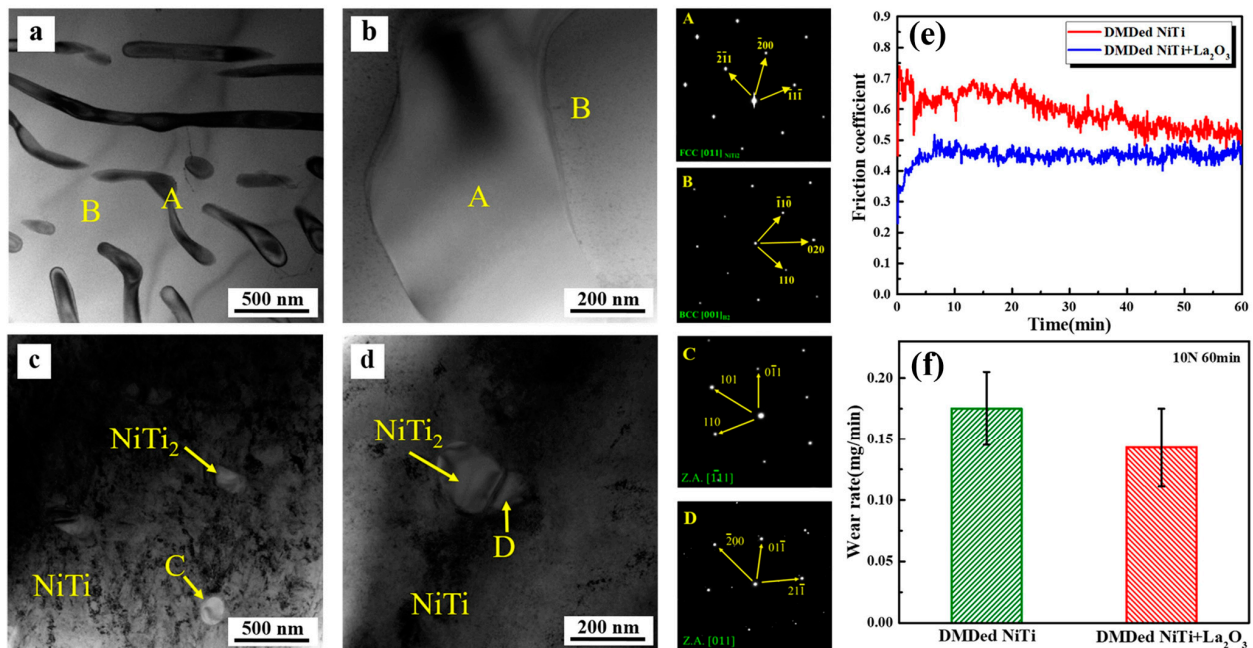


Figure 17. DMD-manufactured NiTi alloy with and without La₂O₃ addition: transmission electron micrographs and selected area electron diffraction (SAED) micrographs. (a,b) NiTi specimens, (c,d) NiTi + La₂O₃, (e) friction coefficients, and (f) wear mass loss. Adapted with permission from Ref. [156]. Copyright 2020 Elsevier. ((A): NiTi₂ phase with an FCC structure; (B): austenite NiTi phase with a BCC structure; (C): one ellipsoidal precipitated phase distributed on the austenite NiTi matrix phase; (D): one spherical precipitated phase connected with NiTi₂ phase).

7. Influence of AM Process Parameters, Post-Process Methods, and Test Parameters

The influence of AM process parameters, post-process methods, and test parameters on AM-manufactured metallic biomaterials is a topic of significant research [158,159]. Several studies have investigated the impact of process parameters on the characteristics of additively manufactured parts, including the optimization of parameters, chamber environment, and post-processing techniques. Additionally, the corrosion and wear behavior of additively manufactured alloys, such as stainless steel, titanium, and aluminum alloys, has been a focus of research, with factors such as laser power, laser scanning, heat treatment, surface polishing, microstructure, porosity, and oxide layer thickness being identified as influential parameters [148,160].

The best corrosion performance and wear performance of additively manufactured (AM) alloys can be influenced by various parameters, including: (i) alloy composition: the choice of alloying elements can significantly impact the corrosion and wear resistance of the material. For example, the addition of Al and Si has been found to improve the wear resistance of a Mg alloy [148]; (ii) AM process parameters: factors such as laser power, laser scanning, and post-processing methods such as heat treatment and surface polishing can influence the microstructure, porosity, and oxide layer thickness of the alloy, which in turn affect corrosion and wear performance [148]; (iii) microstructure: the microstructure of the alloy, including the presence of specific phases or structures, can impact corrosion resistance. For example, the addition of Mn–Si nanoparticles in wrought 316L stainless steel has been shown to reduce pitting susceptibility and improve microstructural anisotropy in SLM-processed parts [160]; (iv) environmental conditions: the corrosion behavior of AM alloys can be influenced by the pH and composition of the surrounding environment, particularly in the presence of chloride ions, which can be detrimental to the durability of various alloys [147]; (v) test parameters: the choice of test parameters, such as the type of corrosion test (e.g., salt spray, immersion, or electrochemical) and the specific conditions

of wear testing (e.g., sliding speed, load, and environment), can impact the assessment of corrosion and wear performance [148].

8. Future Research Directions

Future research should be conducted on complex lattice materials such as triply periodic minimal surfaces, especially on the lattices' internal features and strut deviations and dimensions. Hence, the post-processing surface treatments have a great impact on the behavior and properties of AM parts, so they should be further investigated. Additionally, special attention should be paid to the generation of oxides on alloys' surfaces, sub-surface porosity, roughness, and residual stresses. Although there are numerous studies on the microstructure, grain boundary, and melt-pool boundaries, the effect of various heat treatments and post-processing should still be carefully studied. In addition to the effect of heat treatment, the exact effect of the formation of different phases, their distribution, and morphology should also be carefully examined.

The study of new materials such as high-entropy alloys, multifunctional materials, composites, and Scalma alloys can lead to a better understanding of the exact mechanisms behind the corrosion and tribological behavior of AM parts. In addition to the direct effect of defects, microstructural heterogeneities due to the presence of secondary phases, solute segregation, secondary phase appearance, and grain size variations can change the oxide state and properties and finally affect the tribocorrosion response of AM-manufactured materials. In AM-manufactured biomedical implants, the influence of lubrication mechanisms on the generation and propagation of micro-cracks also needs to be surveyed. Generally, it can be claimed that any non-equilibrium microstructure, secondary phases, etc. can considerably influence the overall properties of AM parts. Hence, it is of crucial importance to control AM variables, parameters, and characterization techniques to comprehend and identify any structure–property mechanisms and relationships. Currently, the addition of various reinforcements to AM materials is a research trend, hence any feature and condition about these should be carefully understood, such as the reinforcement type (continuous, chopped, fibers). Besides reinforcements, the generation of coatings on these alloys along with their nature, morphology, chemical composition, and structure and their influence on the duration and long-term life of biomedical parts also needs more investigation. In brief, consideration of all these points paves the way for scientists to progress toward the development and fabrication of novel biomaterials with various functionalities for implants. Up to now, AM-manufactured titanium and its alloys are highly investigated in the biomedical field since there is a considerable dependency on them, but unfortunately, other metallic systems and alloys are not equally investigated as fully functional materials, such as magnesium that has a unique feature of biodegradability. In this regard, numerous studies should be focused on controlling their corrosion, wear, and biodegradability in order to enhance their performance in the human natural environment, specifically for bone replacements. Until now, no research has yet been reported on Mg powder ceramics as a potential biomaterial for orthopedic applications, while these magnesium powders can be the revolutionary option for lots of orthopedic applications such as bone screws. Finally, it should be noted that the production of AM biomedical components with enhanced corrosion and wear properties can be even more sophisticated through the use of state-of-the-art computational methods, notably, artificial intelligence/deep learning/machine learning/cloud computing. These technologies can be utilized specifically on SLMed and EBMed parts as the most utilized AM methods in this field in order to attain a new generation of novel high-throughput AM-manufactured biomedical components with various beneficial functionalities and enhanced performance.

9. Conclusions

This study concentrated on discussing the corrosion response and tribological behavior of additively manufactured samples for biomedical applications. The AM-based technologies have great potential for dealing with complex geometries, which is very essential for

biomedical implants with intricate and complex geometries and structures. It is certain that the utilization of AM techniques and their related parameters can substantially influence the performance, duration, quality, and functionality of the produced biomedical parts. It is well documented that corrosion and wear still pose a threat to metallic AM-manufactured alloys mainly due to innate process defects, pores, microstructural issues, and heterogeneities. In this regard, the biodegradability of the biomaterial including its corrosion performance and wear behavior plays a key role in its overall performance, preventing any need for secondary surgeries, which are a heavy burden for both the patient and health system. It was reported that surface texturing using AM technologies can have a great impact on the electrochemical response, wear, and tribological behavior, and influence the hydrodynamic pressures. The literature review of the conducted investigations indicates that anodic oxidation is beneficial in metallic components in order to reduce the corrosion rate. There are differences and contradictions between the results obtained in various studies, mainly due to different variables used during AM processing and post-processing, characterization methods, microstructure variations, and defect uncertainties. It was also shown that various surface treatments can lead to surface normalization, surface texture, and a reduction in porosities, which, together may increase the life of a part through, for example, increasing corrosion resistance, fatigue strength, and wear resistance. However, there are limited studies on the impact of other surface treatments such as polishing, magnetic abrasive machining, drag-finishing, vibratory surface finishing, sandblasting, and shot-peening on corrosion and wear performance.

The corrosion and wear performance of AM-manufactured metallic alloys is influenced by various factors, including alloy composition, microstructure, AM process parameters, environmental conditions, and test parameters. The microstructure of AM alloys can vary from traditional techniques, which have an obvious effect on corrosion performance. The choice of alloying elements can significantly impact the corrosion and wear resistance of the material. The AM process parameters, such as laser power, laser scanning, and post-processing methods such as heat treatment and surface polishing, can influence the microstructure, porosity, and oxide layer thickness of the alloy, which in turn affect corrosion and wear performance. The environmental conditions, such as pH and composition of the surrounding environment, can also impact the corrosion behavior of AM alloys. The choice of test parameters, such as the type of corrosion test and the specific conditions of wear testing, can impact the assessment of corrosion and wear performance. In summary, optimizing alloy composition, microstructure, AM process parameters, environmental conditions, and test parameters can help achieve the best corrosion and wear performance of AM metallic alloys for specific applications. Further research is needed to identify the optimal conditions and parameters for each alloy system, taking into account the unique properties and requirements of the application.

Author Contributions: Conceptualization, Z.W. and S.A.; methodology, S.A.; software, J.L.; validation, Z.W., S.A. and M.E.; formal analysis, S.A.; investigation, Z.W., S.A. and J.L.; resources, M.E.; writing—original draft preparation, Z.W., S.A. and M.E.; writing—review and editing, Z.W., S.A. and M.E.; visualization, J.L.; supervision, M.E.; project administration, M.E.; funding acquisition, S.A. and M.E. All authors have read and agreed to the published version of the manuscript.

Funding: This research received no external funding.

Data Availability Statement: Not applicable.

Conflicts of Interest: The authors declare no conflict of interest.

References

1. Aaryashree; Shinde, P.V.; Kumar, A.; Late, D.J.; Rout, C.S. Recent advances in 2D black phosphorus based materials for gas sensing applications. *J. Mater. Chem. C* **2021**, *9*, 3773–3794. [[CrossRef](#)]
2. Sheoran, A.J.; Kumar, H.; Arora, P.K.; Moona, G. Bio-Medical applications of Additive Manufacturing: A Review. *Procedia Manuf.* **2020**, *51*, 663–670. [[CrossRef](#)]

3. Attarilar, S.; Ebrahimi, M.; Djevanroodi, F.; Fu, Y.; Wang, L.; Yang, J. 3D Printing Technologies in Metallic Implants: A Thematic Review on the Techniques and Procedures. *Int. J. Bioprint.* **2021**, *7*, 306. [[CrossRef](#)]
4. Ashish; Ahmad, N.; Gopinath, P.; Vinogradov, A. 3D Printing in Medicine. In *3D Printing Technology in Nanomedicine*; Elsevier: Amsterdam, The Netherlands, 2019; pp. 1–22.
5. Shirazi, S.F.S.; Gharekhani, S.; Mehrali, M.; Yarmand, H.; Metselaar, H.S.C.; Adib Kadri, N.; Osman, N.A.A. A review on powder-based additive manufacturing for tissue engineering: Selective laser sintering and inkjet 3D printing. *Sci. Technol. Adv. Mater.* **2015**, *16*, 033502. [[CrossRef](#)] [[PubMed](#)]
6. Wang, Y.; Zhai, W.; Cheng, S.; Li, J.; Zhang, H. Surface-functionalized design of blood-contacting biomaterials for preventing coagulation and promoting hemostasis. *Friction* **2023**, *11*, 1371–1394. [[CrossRef](#)]
7. Criaes, L.E.; Arisoy, Y.M.; Lane, B.; Moylan, S.; Donmez, A.; Özel, T. Laser powder bed fusion of nickel alloy 625: Experimental investigations of effects of process parameters on melt pool size and shape with spatter analysis. *Int. J. Mach. Tools Manuf.* **2017**, *121*, 22–36. [[CrossRef](#)]
8. Ventola, C.L. Medical Applications for 3D Printing: Current and Projected Uses. *Pharm. Ther.* **2014**, *39*, 704–711.
9. Sinha, S.K. Additive manufacturing (AM) of medical devices and scaffolds for tissue engineering based on 3D and 4D printing. In *3D and 4D Printing of Polymer Nanocomposite Materials*; Elsevier: Amsterdam, The Netherlands, 2020; pp. 119–160.
10. Xiang, G.; Yang, T.; Guo, J.; Wang, J.; Liu, B.; Chen, S. Optimization Transient Wear and Contact Performances of Water-Lubricated Bearings under Fluid-Solid-Thermal Coupling Condition Using Profile Modification. *Wear* **2022**, *502–503*, 204379. [[CrossRef](#)]
11. Wang, N.X.; Wang, Y.S.; Zheng, K.; Zhi, J.Q.; Zhou, B.; Wu, Y.X.; Xue, Y.P.; Ma, Y.; Cheng, F.; Gao, J.; et al. Achieving CVD Diamond Films on Mo_{0.5}(TiZrTaW)_{0.5} Highly Concentrated Alloy for Ultrastrong Corrosion Resistance. *Surf. Coat. Technol.* **2023**, *466*, 129620. [[CrossRef](#)]
12. Mazzoni, S.; Bianchi, A.; Schiariti, G.; Badiali, G.; Marchetti, C. Computer-Aided Design and Computer-Aided Manufacturing Cutting Guides and Customized Titanium Plates Are Useful in Upper Maxilla Waferless Repositioning. *J. Oral Maxillofac. Surg.* **2015**, *73*, 701–707. [[CrossRef](#)]
13. Buijs, G.J.; van Bakelen, N.B.; Jansma, J.; de Visscher, J.G.A.M.; Hoppenreijns, T.J.M.; Bergsma, J.E.; Stegenga, B.; Bos, R.R.M. A Randomized Clinical Trial of Biodegradable and Titanium Fixation Systems in Maxillofacial Surgery. *J. Dent. Res.* **2012**, *91*, 299–304. [[CrossRef](#)] [[PubMed](#)]
14. Staiger, M.P.; Pietak, A.M.; Huadmai, J.; Dias, G. Magnesium and its alloys as orthopedic biomaterials: A review. *Biomaterials* **2006**, *27*, 1728–1734. [[CrossRef](#)]
15. Ebrahimi, M.; Wang, Q.; Attarilar, S. A comprehensive review of magnesium-based alloys and composites processed by cyclic extrusion compression and the related techniques. *Prog. Mater. Sci.* **2023**, *131*, 101016. [[CrossRef](#)]
16. Liao, D.; Zhu, S.-P.; Keshtegar, B.; Qian, G.; Wang, Q. Probabilistic framework for fatigue life assessment of notched components under size effects. *Int. J. Mech. Sci.* **2020**, *181*, 105685. [[CrossRef](#)]
17. Gode, C.; Attarilar, S.; Eghbali, B.; Ebrahimi, M. Electrochemical behavior of equal channel angular pressed titanium for biomedical application. *AIP Conf. Proc.* **2015**, *1653*, 020041.
18. Zhang, Y.; Attarilar, S.; Wang, L.; Lu, W.; Yang, J.; Fu, Y. A Review on Design and Mechanical Properties of Additively Manufactured NiTi Implants for Orthopedic Applications. *Int. J. Bioprint.* **2021**, *7*, 340. [[CrossRef](#)] [[PubMed](#)]
19. Attarilar, S.; Salehi, M.T.; Al-Fadhalah, K.J.; Djevanroodi, F.; Mozafari, M. Functionally graded titanium implants: Characteristic enhancement induced by combined severe plastic deformation. *PLoS ONE* **2019**, *14*, e0221491. [[CrossRef](#)]
20. Turnbull, G.; Clarke, J.; Picard, F.; Riches, P.; Jia, L.; Han, F.; Li, B.; Shu, W. 3D Bioactive Composite Scaffolds for Bone Tissue Engineering. *Bioact. Mater.* **2018**, *3*, 278–314. [[CrossRef](#)]
21. Liu, J.; Zhou, Y.; Lu, J.; Cai, R.; Zhao, T.; Chen, Y.; Zhang, M.; Lu, X.; Chen, Y. Injectable, tough and adhesive zwitterionic hydrogels for 3D-printed wearable strain sensors. *Chem. Eng. J.* **2023**, *475*, 146340. [[CrossRef](#)]
22. Derakhshanfar, S.; Mbeleck, R.; Xu, K.; Zhang, X.; Zhong, W.; Xing, M. 3D bioprinting for biomedical devices and tissue engineering: A review of recent trends and advances. *Bioact. Mater.* **2018**, *3*, 144–156. [[CrossRef](#)]
23. Nagarajan, N.; Dupret-Bories, A.; Karabulut, E.; Zorlutuna, P.; Vrana, N.E. Enabling personalized implant and controllable biosystem development through 3D printing. *Biotechnol. Adv.* **2018**, *36*, 521–533. [[CrossRef](#)] [[PubMed](#)]
24. Do, A.-V.; Smith, R.; Aciri, T.M.; Geary, S.M.; Salem, A.K. 3D printing technologies for 3D scaffold engineering. In *Functional 3D Tissue Engineering Scaffolds*; Elsevier: Amsterdam, The Netherlands, 2018; pp. 203–234.
25. Niu, X.; Zhu, S.-P.; He, J.-C.; Liao, D.; Correia, J.A.F.O.; Berto, F.; Wang, Q. Defect tolerant fatigue assessment of AM materials: Size effect and probabilistic prospects. *Int. J. Fatigue* **2022**, *160*, 106884. [[CrossRef](#)]
26. Attarilar, S.; Yang, J.; Ebrahimi, M.; Wang, Q.; Liu, J.; Tang, Y.; Yang, J. The Toxicity Phenomenon and the Related Occurrence in Metal and Metal Oxide Nanoparticles: A Brief Review From the Biomedical Perspective. *Front. Bioeng. Biotechnol.* **2020**, *8*. [[CrossRef](#)] [[PubMed](#)]
27. Souza, J.C.M.; Henriques, M.; Teughels, W.; Ponthiaux, P.; Celis, J.-P.; Rocha, L.A. Wear and Corrosion Interactions on Titanium in Oral Environment: Literature Review. *J. Bio-Tribo-Corrosion* **2015**, *1*, 13. [[CrossRef](#)]
28. Manivasagam, G.; Dhinasekaran, D.; Rajamanickam, A. Biomedical Implants: Corrosion and its Prevention—A Review. *Recent Patents Corros. Sci.* **2010**, *2*, 40–54. [[CrossRef](#)]
29. Aksakal, B.; Yildirim, Ö.S.; Gul, H. Metallurgical failure analysis of various implant materials used in orthopedic applications. *J. Fail. Anal. Prev.* **2004**, *4*, 17–23. [[CrossRef](#)]

30. Xu, J.; Chang, L.; Chen, T.; Ren, T.; Zhang, Y.; Cai, Z. Study of the bending properties of variable stiffness chain mail fabrics. *Compos. Struct.* **2023**, *322*, 117369. [[CrossRef](#)]
31. Huang, X.; Chang, L.; Zhao, H.; Cai, Z. Study on craniocerebral dynamics response and helmet protective performance under the blast waves. *Mater. Des.* **2022**, *224*, 111408. [[CrossRef](#)]
32. Attarilar, S.; Djavanroodi, F.; Irfan, O.M.; Al-Mufadi, F.A.; Ebrahimi, M.; Wang, Q.D. Strain uniformity footprint on mechanical performance and erosion-corrosion behavior of equal channel angular pressed pure titanium. *Results Phys.* **2020**, *17*, 103141. [[CrossRef](#)]
33. Fan, R.-j.; Attarilar, S.; Shamsborhan, M.; Ebrahimi, M.; Göde, C.; Özkavak, H.V. Enhancing mechanical properties and corrosion performance of AA6063 aluminum alloys through constrained groove pressing technique. *Trans. Nonferrous Met. Soc. China* **2020**, *30*, 1790–1802. [[CrossRef](#)]
34. Badkoobeh, F.; Mostaan, H.; Rafiei, M.; Bakhsheshi-Rad, H.R.; RamaKrishna, S.; Chen, X. Additive manufacturing of biodegradable magnesium-based materials: Design strategies, properties, and biomedical applications. *J. Magnes. Alloys* **2023**, *11*, 801–839. [[CrossRef](#)]
35. Pandey, A.K.; Gautam, R.K.; Behera, C.K. Corrosion and wear behavior of Ti–5Cu–xNb biomedical alloy in simulated body fluid for dental implant applications. *J. Mech. Behav. Biomed. Mater.* **2023**, *137*, 105533. [[CrossRef](#)] [[PubMed](#)]
36. Mahajan, A.; Singh, G.; Devgan, S. Additive manufacturing of metallic biomaterials: A concise review. *Arch. Civ. Mech. Eng.* **2023**, *23*, 187. [[CrossRef](#)]
37. Markhoff, J.; Grabow, N. Wear and corrosion in medical applications. *Curr. Dir. Biomed. Eng.* **2020**, *6*, 434–437. [[CrossRef](#)]
38. Jiang, X.J.; Bao, S.J.; Zhang, L.W.; Zhang, X.Y.; Jiao, L.S.; Qi, H.B.; Wang, F. Effect of Zr on microstructure and properties of TC4 alloy fabricated by laser additive manufacturing. *J. Mater. Res. Technol.* **2023**, *24*, 8782–8792. [[CrossRef](#)]
39. Lin, B.; Yang, K.; Bao, X.; Liu, J.; Guo, Q.; Zhang, L.; Wang, Q.; Hua, N. Enhanced wear, corrosion, and corrosive-wear resistance of the biocompatible Ti-based bulk metallic glass by oxidation treatment. *J. Non. Cryst. Solids* **2022**, *576*, 121231. [[CrossRef](#)]
40. Yadav, D.; Garg, R.K.; Ahlawat, A.; Chhabra, D. 3D printable biomaterials for orthopedic implants: Solution for sustainable and circular economy. *Resour. Policy* **2020**, *68*, 101767. [[CrossRef](#)]
41. Gorsse, S.; Hutchinson, C.; Gouné, M.; Banerjee, R. Additive manufacturing of metals: A brief review of the characteristic microstructures and properties of steels, Ti-6Al-4V and high-entropy alloys. *Sci. Technol. Adv. Mater.* **2017**, *18*, 584–610. [[CrossRef](#)]
42. Saeidi, K.; Gao, X.; Zhong, Y.; Shen, Z.J. Hardened austenite steel with columnar sub-grain structure formed by laser melting. *Mater. Sci. Eng. A* **2015**, *625*, 221–229. [[CrossRef](#)]
43. Luo, S.; Gao, P.; Yu, H.; Yang, J.; Wang, Z.; Zeng, X. Selective laser melting of an equiatomic AlCrCuFeNi high-entropy alloy: Processability, non-equilibrium microstructure and mechanical behavior. *J. Alloys Compd.* **2019**, *771*, 387–397. [[CrossRef](#)]
44. Chen, S.; Li, Y.; Zhi, S.; Ding, Z.; Huang, Y.; Wang, W.; Zheng, R.; Yu, H.; Wang, J.; Hu, M.; et al. lncRNA Xist Regulates Osteoblast Differentiation by Sponging miR-19a-3p in Aging-induced Osteoporosis. *Aging Dis.* **2020**, *11*, 1058. [[CrossRef](#)] [[PubMed](#)]
45. Shifeng, W.; Shuai, L.; Qingsong, W.; Yan, C.; Sheng, Z.; Yusheng, S. Effect of molten pool boundaries on the mechanical properties of selective laser melting parts. *J. Mater. Process. Technol.* **2014**, *214*, 2660–2667. [[CrossRef](#)]
46. Ganesh, P.; Giri, R.; Kaul, R.; Ram Sankar, P.; Tiwari, P.; Atulkar, A.; Porwal, R.K.; Dayal, R.K.; Kukreja, L.M. Studies on pitting corrosion and sensitization in laser rapid manufactured specimens of type 316L stainless steel. *Mater. Des.* **2012**, *39*, 509–521. [[CrossRef](#)]
47. Otero, E.; Pardo, A.; Utrilla, M.V.; Sáenz, E.; Perez, F.J. Influence of microstructure on the corrosion resistance of AISI type 304L and type 316L sintered stainless steels exposed to ferric chloride solution. *Mater. Charact.* **1995**, *35*, 145–151. [[CrossRef](#)]
48. Ebrahimi, M.; Attarilar, S.; Shaeri, M.H.; Gode, C.; Armoon, H.; Djavanroodi, F. An investigation into the effect of alloying elements on corrosion behavior of severely deformed Cu-Sn alloys by equal channel angular pressing. *Arch. Civ. Mech. Eng.* **2019**, *19*, 842–850. [[CrossRef](#)]
49. Revilla, R.; Verkens, D.; Rubben, T.; De Graeve, I. Corrosion and Corrosion Protection of Additively Manufactured Aluminium Alloys—A Critical Review. *Materials* **2020**, *13*, 4804. [[CrossRef](#)] [[PubMed](#)]
50. Kempen, K.; Thijs, L.; Van Humbeeck, J.; Kruth, J.-P. Processing AlSi10Mg by selective laser melting: Parameter optimisation and material characterisation. *Mater. Sci. Technol.* **2015**, *31*, 917–923. [[CrossRef](#)]
51. Carter, L.N.; Essa, K.; Attallah, M.M. Optimisation of selective laser melting for a high temperature Ni-superalloy. *Rapid Prototyp. J.* **2015**, *21*, 423–432. [[CrossRef](#)]
52. Karakurt, I.; Lin, L. 3D printing technologies: Techniques, materials, and post-processing. *Curr. Opin. Chem. Eng.* **2020**, *28*, 134–143. [[CrossRef](#)]
53. Geenen, K.; Röttger, A.; Theisen, W. Corrosion behavior of 316L austenitic steel processed by selective laser melting, hot-isostatic pressing, and casting. *Mater. Corros.* **2017**, *68*, 764–775. [[CrossRef](#)]
54. Boschetto, A.; Bottini, L.; Veniali, F. Roughness modeling of AlSi10Mg parts fabricated by selective laser melting. *J. Mater. Process. Technol.* **2017**, *241*, 154–163. [[CrossRef](#)]
55. Tian, Y.; Tomus, D.; Rometsch, P.; Wu, X. Influences of processing parameters on surface roughness of Hastelloy X produced by selective laser melting. *Addit. Manuf.* **2017**, *13*, 103–112. [[CrossRef](#)]
56. Prando, D.; Brenna, A.; Diamanti, M.V.; Beretta, S.; Bolzoni, F.; Ormellese, M.; Pedefferri, M. Corrosion of titanium: Part 2: Effects of surface treatments. *J. Appl. Biomater. Funct. Mater.* **2018**, *16*, 3–13. [[CrossRef](#)] [[PubMed](#)]

57. Croll, S.G. Surface roughness profile and its effect on coating adhesion and corrosion protection: A review. *Prog. Org. Coat.* **2020**, *148*, 105847. [[CrossRef](#)]
58. Zuo, Y.; Wang, H.; Xiong, J. The aspect ratio of surface grooves and metastable pitting of stainless steel. *Corros. Sci.* **2002**, *44*, 25–35. [[CrossRef](#)]
59. Shahryari, A.; Kamal, W.; Omanovic, S. The effect of surface roughness on the efficiency of the cyclic potentiodynamic passivation (CPP) method in the improvement of general and pitting corrosion resistance of 316LVM stainless steel. *Mater. Lett.* **2008**, *62*, 3906–3909. [[CrossRef](#)]
60. Kong, D.; Dong, C.; Ni, X.; Man, C.; Xiao, K.; Li, X. Insight into the mechanism of alloying elements (Sn, Be) effect on copper corrosion during long-term degradation in harsh marine environment. *Appl. Surf. Sci.* **2018**, *455*, 543–553. [[CrossRef](#)]
61. Walter, R.; Kannan, M.B. Influence of surface roughness on the corrosion behaviour of magnesium alloy. *Mater. Des.* **2011**, *32*, 2350–2354. [[CrossRef](#)]
62. Bossis, P.; Lefebvre, F.; Barb eris, P.; Galerie, A. Corrosion of Zirconium Alloys: Link between the Metal/Oxide Interface Roughness, the Degradation of the Protective Oxide Layer and the Corrosion Kinetics. *Mater. Sci. Forum* **2001**, *369–372*, 255–262. [[CrossRef](#)]
63. Wu, J.; Djavanroodi, F.; Shamsborhan, M.; Attarilar, S.; Ebrahimi, M. Improving Mechanical and Corrosion Behavior of 5052 Aluminum Alloy Processed by Cyclic Extrusion Compression. *Metals* **2022**, *12*, 1288. [[CrossRef](#)]
64. Xu, G.; Wang, K.; Dong, X.; Yang, L.; Ebrahimi, M.; Jiang, H.; Wang, Q.; Ding, W. Review on corrosion resistance of mild steels in liquid aluminum. *J. Mater. Sci. Technol.* **2021**, *71*, 12–22. [[CrossRef](#)]
65. Chen, S.Y.; Huang, J.C.; Pan, C.T.; Lin, C.H.; Yang, T.L.; Huang, Y.S.; Ou, C.H.; Chen, L.Y.; Lin, D.Y.; Lin, H.K.; et al. Microstructure and mechanical properties of open-cell porous Ti-6Al-4V fabricated by selective laser melting. *J. Alloys Compd.* **2017**, *713*, 248–254. [[CrossRef](#)]
66. Rezaie, F.; Farshbaf, M.; Dahri, M.; Masjedi, M.; Maleki, R.; Amini, F.; Wirth, J.; Moharamzadeh, K.; Weber, F.E.; Tayebi, L. 3D Printing of Dental Prostheses: Current and Emerging Applications. *J. Compos. Sci.* **2023**, *7*, 80. [[CrossRef](#)]
67. Yao, Q.; Morton, D.; Eckert, G.J.; Lin, W.-S. The effect of surface treatments on the color stability of CAD-CAM interim fixed dental prostheses. *J. Prosthet. Dent.* **2021**, *126*, 248–253. [[CrossRef](#)] [[PubMed](#)]
68. Ebrahimi, M.; Gode, C.; Attarilar, S.; Berjis, R. Concurrent Enhancement of Strength and Corrosion Resistance in Ultrafine-grained Al6063 Tubes. *Trans. Indian Inst. Met.* **2021**, *74*, 753–766. [[CrossRef](#)]
69. Djavanroodi, F.; Ebrahimi, M.; Nayfeh, J.F. Tribological and mechanical investigation of multi-directional forged nickel. *Sci. Rep.* **2019**, *9*, 241. [[CrossRef](#)]
70. Wu, M.-W.; Lai, P.-H.; Chen, J.-K. Anisotropy in the impact toughness of selective laser melted Ti-6Al-4V alloy. *Mater. Sci. Eng. A* **2016**, *650*, 295–299. [[CrossRef](#)]
71. Kok, Y.; Tan, X.P.; Wang, P.; Nai, M.L.S.; Loh, N.H.; Liu, E.; Tor, S.B. Anisotropy and heterogeneity of microstructure and mechanical properties in metal additive manufacturing: A critical review. *Mater. Des.* **2018**, *139*, 565–586. [[CrossRef](#)]
72. Chen, Y.; Zhang, J.; Gu, X.; Dai, N.; Qin, P.; Zhang, L.-C. Distinction of corrosion resistance of selective laser melted Al-12Si alloy on different planes. *J. Alloys Compd.* **2018**, *747*, 648–658. [[CrossRef](#)]
73. Feliu, S. Electrochemical Impedance Spectroscopy for the Measurement of the Corrosion Rate of Magnesium Alloys: Brief Review and Challenges. *Metals* **2020**, *10*, 775. [[CrossRef](#)]
74. Revilla, R.I.; Wouters, B.; Andreatta, F.; Lanzutti, A.; Fedrizzi, L.; De Graeve, I. EIS comparative study and critical Equivalent Electrical Circuit (EEC) analysis of the native oxide layer of additive manufactured and wrought 316L stainless steel. *Corros. Sci.* **2020**, *167*, 108480. [[CrossRef](#)]
75. Egorkin, V.S.; Medvedev, I.M.; Sinebryukhov, S.L.; Vyalii, I.E.; Gnedenkov, A.S.; Nadaraia, K.V.; Izotov, N.V.; Mashtalyar, D.V.; Gnedenkov, S.V. Atmospheric and Marine Corrosion of PEO and Composite Coatings Obtained on Al-Cu-Mg Aluminum Alloy. *Materials* **2020**, *13*, 2739. [[CrossRef](#)] [[PubMed](#)]
76. Wei, B.; Xu, J.; Pang, J.; Huang, Z.; Wu, J.; Cai, Z.; Yan, M.; Sun, C. Prediction of electrochemical impedance spectroscopy of high-entropy alloys corrosion by using gradient boosting decision tree. *Mater. Today Commun.* **2022**, *32*, 104047. [[CrossRef](#)]
77. Zhao, D.; Chen, D.; Feng, X.; Chen, Z.; Jin, C.; Tan, X.; Xiang, Y.; Jiao, W.; Fang, Y.; Xu, L.; et al. Bioactive coating with antibacterial and anticorrosive properties deposited on ZA6-1 alloy bone implant. *Trans. Nonferrous Met. Soc. China* **2023**, *33*, 1507–1521. [[CrossRef](#)]
78. Gnedenkov, A.S.; Sinebryukhov, S.L.; Filonina, V.S.; Ustinov, A.Y.; Gnedenkov, S.V. Hybrid Coatings for Active Protection against Corrosion of Mg and Its Alloys. *Polymers* **2023**, *15*, 3035. [[CrossRef](#)] [[PubMed](#)]
79. Muresan, L.M. Nanocomposite Coatings for Anti-Corrosion Properties of Metallic Substrates. *Materials* **2023**, *16*, 5092. [[CrossRef](#)] [[PubMed](#)]
80. Acquesta, A.; Russo, P.; Monetta, T. Plasma Electrolytic Oxidation Treatment of AZ31 Magnesium Alloy for Biomedical Applications: The Influence of Applied Current on Corrosion Resistance and Surface Characteristics. *Crystals* **2023**, *13*, 510. [[CrossRef](#)]
81. Nahum, E.Z.; Lugovskoy, A.; Lugovskoy, S.; Sobolev, A. Synthesis of Titanium Oxide Nanotubes Loaded with Hydroxyapatite. *Nanomaterials* **2023**, *13*, 2743. [[CrossRef](#)]
82. Zeng, Z.; Choudhary, S.; Esmaily, M.; Benn, F.; Derra, T.; Hora, Y.; Kopp, A.; Allanore, A.; Birbilis, N. An additively manufactured magnesium-aluminium alloy withstands seawater corrosion. *npj Mater. Degrad.* **2022**, *6*, 32. [[CrossRef](#)]
83. Karunakaran, R.; Ortgies, S.; Tamayol, A.; Bobaru, F.; Sealy, M.P. Additive manufacturing of magnesium alloys. *Bioact. Mater.* **2020**, *5*, 44–54. [[CrossRef](#)]

84. Wang, H.; Qiang, L.; Mi, X.; Wang, T.; Xu, X. Additive manufacturing of degradable magnesium alloys and their application in orthopedic implants. *Digit. Med.* **2023**, *9*, e00008.
85. Wang, X.; Wen, C. Corrosion protection of mesoporous bioactive glass coating on biodegradable magnesium. *Appl. Surf. Sci.* **2014**, *303*, 196–204. [[CrossRef](#)]
86. Sarian, M.N.; Iqbal, N.; Sotoudehbagha, P.; Razavi, M.; Ahmed, Q.U.; Sukotjo, C.; Hermawan, H. Potential bioactive coating system for high-performance absorbable magnesium bone implants. *Bioact. Mater.* **2022**, *12*, 42–63. [[CrossRef](#)] [[PubMed](#)]
87. García, C.; Ceré, S.; Durán, A. Bioactive coatings deposited on titanium alloys. *J. Non. Cryst. Solids* **2006**, *352*, 3488–3495. [[CrossRef](#)]
88. Coelho, M.F.C.; de Sousa, L.L.; Ferreira, C.C.; Gaspar de Souza, B.F.; Rigo, E.C.d.S.; Mariano, N.A. Biomimetic coating on titanium: Evaluation of bioactivity and corrosion. *Mater. Res. Express* **2020**, *6*, 1265g5. [[CrossRef](#)]
89. George, J.S.; Vijayan, P.P.; Hoang, A.T.; Kalarikkal, N.; Nguyen-Tri, P.; Thomas, S. Recent advances in bio-inspired multifunctional coatings for corrosion protection. *Prog. Org. Coat.* **2022**, *168*, 106858. [[CrossRef](#)]
90. Bhadauria, N.; Pandey, S.; Pandey, P.M. Wear and enhancement of wear resistance—A review. *Mater. Today Proc.* **2020**, *26*, 2986–2991. [[CrossRef](#)]
91. Kumar, A.; Choudhary, A.; Tiwari, A.; James, C.; Kumar, H.; Kumar Arora, P.; Akhtar Khan, S. An investigation on wear characteristics of additive manufacturing materials. *Mater. Today Proc.* **2021**, *47*, 3654–3660. [[CrossRef](#)]
92. Palanisamy, C.; Raman, R. Tribology of additively manufactured materials: Fundamentals, modeling, and applications. In *Tribology of Additively Manufactured Materials*; Elsevier: Amsterdam, The Netherlands, 2022; pp. 223–266.
93. Behrens, B.-A.; Bouguecha, A.; Vucetic, M.; Chugreev, A. Advanced Wear Simulation for Bulk Metal Forming Processes. In *MATEC Web of Conferences, Proceedings of the 12th International Conference on Numerical Methods in Industrial Forming Processes, Troyes, France, 4–7 July 2016*; EDP Sciences: Les Ulis, France, 2016; Volume 80, p. 04003. [[CrossRef](#)]
94. Kessler, A.; Reymus, M.; Hickel, R.; Kunzelmann, K.-H. Three-body wear of 3D printed temporary materials. *Dent. Mater.* **2019**, *35*, 1805–1812. [[CrossRef](#)]
95. Mayer, J.; Stawarczyk, B.; Vogt, K.; Hickel, R.; Edelhoff, D.; Reymus, M. Influence of cleaning methods after 3D printing on two-body wear and fracture load of resin-based temporary crown and bridge material. *Clin. Oral Investig.* **2021**, *25*, 5987–5996. [[CrossRef](#)]
96. Firlej, M.; Pieniak, D.; Niewczas, A.M.; Walczak, A.; Domagała, I.; Borucka, A.; Przystupa, K.; Igielska-Kalwat, J.; Jarosz, W.; Biedziak, B. Effect of Artificial Aging on Mechanical and Tribological Properties of CAD/CAM Composite Materials Used in Dentistry. *Materials* **2021**, *14*, 4678. [[CrossRef](#)] [[PubMed](#)]
97. Li, S.; Li, X.; Hou, W.; Nune, K.C.; Misra, R.D.K.; Correa-Rodriguez, V.L.; Guo, Z.; Hao, Y.; Yang, R.; Murr, L.E. Fabrication of open-cellular (porous) titanium alloy implants: Osseointegration, vascularization and preliminary human trials. *Sci. China Mater.* **2018**, *61*, 525–536. [[CrossRef](#)]
98. Lee, J.T.Y.; Leng, Y.; Chow, K.L.; Ren, F.; Ge, X.; Wang, K.; Lu, X. Cell culture medium as an alternative to conventional simulated body fluid. *Acta Biomater.* **2011**, *7*, 2615–2622. [[CrossRef](#)] [[PubMed](#)]
99. Tjandra, J.; Alabort, E.; Barba, D.; Pedrazzini, S. Corrosion, fatigue and wear of additively manufactured Ti alloys for orthopaedic implants. *Mater. Sci. Technol.* **2023**, *39*, 2951–2965. [[CrossRef](#)]
100. Niinomi, M.; Boehlert, C.J. Titanium Alloys for Biomedical Applications. In *Advances in Metallic Biomaterials*; Springer: Berlin/Heidelberg, Germany, 2015; pp. 179–213. ISBN 978-3-662-46836-4.
101. Li, Y.; Yang, C.; Zhao, H.; Qu, S.; Li, X.; Li, Y. New Developments of Ti-Based Alloys for Biomedical Applications. *Materials* **2014**, *7*, 1709–1800. [[CrossRef](#)] [[PubMed](#)]
102. Elias, C.N.; Lima, J.H.C.; Valiev, R.; Meyers, M.A. Biomedical applications of titanium and its alloys. *JOM* **2008**, *60*, 46–49. [[CrossRef](#)]
103. Sarraf, M.; Rezvani Ghomi, E.; Alipour, S.; Ramakrishna, S.; Liana Sukiman, N. A state-of-the-art review of the fabrication and characteristics of titanium and its alloys for biomedical applications. *Bio-Design Manuf.* **2022**, *5*, 371–395. [[CrossRef](#)] [[PubMed](#)]
104. Xu, J.; Zhang, J.; Shi, Y.; Tang, J.; Huang, D.; Yan, M.; Dargusch, M.S. Surface Modification of Biomedical Ti and Ti Alloys: A Review on Current Advances. *Materials* **2022**, *15*, 1749. [[CrossRef](#)]
105. Chen, S.Y.; Kuo, C.N.; Su, Y.L.; Huang, J.C.; Wu, Y.C.; Lin, Y.H.; Chung, Y.C.; Ng, C.H. Microstructure and fracture properties of open-cell porous Ti-6Al-4V with high porosity fabricated by electron beam melting. *Mater. Charact.* **2018**, *138*, 255–262. [[CrossRef](#)]
106. Ataee, A.; Li, Y.; Fraser, D.; Song, G.; Wen, C. Anisotropic Ti-6Al-4V gyroid scaffolds manufactured by electron beam melting (EBM) for bone implant applications. *Mater. Des.* **2018**, *137*, 345–354. [[CrossRef](#)]
107. Seah, K.H.W.; Thampuran, R.; Teoh, S.H. The influence of pore morphology on corrosion. *Corros. Sci.* **1998**, *40*, 547–556. [[CrossRef](#)]
108. Li, Y.X.; Cui, Z.D.; Yang, X.J.; Zhu, S.L. Corrosion Behavior of Porous Ti-24Nb-4Zr Alloy in Different Simulated Body Fluids. *Adv. Mater. Res.* **2011**, *399–401*, 1577–1581. [[CrossRef](#)]
109. Menini, R.; Dion, M.-J.; So, S.K.V.; Gauthier, M.; Lefebvre, L.-P. Surface and Corrosion Electrochemical Characterization of Titanium Foams for Implant Applications. *J. Electrochem. Soc.* **2006**, *153*, B13. [[CrossRef](#)]
110. Blackwood, D.; Chooi, S.K. Stability of protective oxide films formed on a porous titanium. *Corros. Sci.* **2002**, *44*, 395–405. [[CrossRef](#)]

111. Morris, D.; Mamidi, S.K.; Kamat, S.; Cheng, K.; Bijukumar, D.; Tsai, P.-I.; Wu, M.-H.; Oriás, A.A.E.; Mathew, M.T. Mechanical, Electrochemical and Biological Behavior of 3D Printed-Porous Titanium for Biomedical Applications. *J. Bio- Tribo-Corrosion* **2021**, *7*, 39. [[CrossRef](#)]
112. Sharp, R.; Pelletier, M.H.; Walsh, W.R.; Kelly, C.N.; Gall, K. Corrosion Resistance of 3D Printed Ti6Al4V Gyroid Lattices with Varying Porosity. *Materials* **2022**, *15*, 4805. [[CrossRef](#)] [[PubMed](#)]
113. Zhao, X.; Li, S.; Zhang, M.; Liu, Y.; Sercombe, T.B.; Wang, S.; Hao, Y.; Yang, R.; Murr, L.E. Comparison of the microstructures and mechanical properties of Ti–6Al–4V fabricated by selective laser melting and electron beam melting. *Mater. Des.* **2016**, *95*, 21–31. [[CrossRef](#)]
114. Gai, X.; Bai, Y.; Li, S.; Wang, L.; Ai, S.; Hao, Y.; Yang, R.; Dai, K. Review on Corrosion Characteristics of Porous Titanium Alloys Fabricated by Additive Manufacturing. *J. Shanghai Jiaotong Univ.* **2021**, *26*, 416–430. [[CrossRef](#)]
115. Zhou, L.; Yuan, T.; Tang, J.; He, J.; Li, R. Mechanical and corrosion behavior of titanium alloys additively manufactured by selective laser melting—A comparison between nearly β titanium, α titanium and $\alpha + \beta$ titanium. *Opt. Laser Technol.* **2019**, *119*, 105625. [[CrossRef](#)]
116. Oliveira, N.T.C.; Ferreira, E.A.; Duarte, L.T.; Biaggio, S.R.; Rocha-Filho, R.C.; Bocchi, N. Corrosion resistance of anodic oxides on the Ti–50Zr and Ti–13Nb–13Zr alloys. *Electrochim. Acta* **2006**, *51*, 2068–2075. [[CrossRef](#)]
117. Pede, D.; Li, M.; Virovac, L.; Poleske, T.; Balle, F.; Müller, C.; Mozaffari-Jovein, H. Microstructure and corrosion resistance of novel β -type titanium alloys manufactured by selective laser melting. *J. Mater. Res. Technol.* **2022**, *19*, 4598–4612. [[CrossRef](#)]
118. Liang, Z.; Tang, B.; Gui, Y.; Zhao, Q. Corrosion resistance of 3D-printed and cold-rolled titanium alloys at 600 °C in air and air-SO₂ environments. *Mater. Today Commun.* **2020**, *24*, 101055. [[CrossRef](#)]
119. Gai, X.; Bai, Y.; Li, J.; Li, S.; Hou, W.; Hao, Y.; Zhang, X.; Yang, R.; Misra, R.D.K. Electrochemical behaviour of passive film formed on the surface of Ti-6Al-4V alloys fabricated by electron beam melting. *Corros. Sci.* **2018**, *145*, 80–89. [[CrossRef](#)]
120. Ralston, K.D.; Birbilis, N.; Davies, C.H.J. Revealing the relationship between grain size and corrosion rate of metals. *Scr. Mater.* **2010**, *63*, 1201–1204. [[CrossRef](#)]
121. Zhang, L.J.; Fan, J.J.; Zhang, Z.; Cao, F.H.; Zhang, J.Q.; Cao, C.N. Study on the anodic film formation process of AZ91D magnesium alloy. *Electrochim. Acta* **2007**, *52*, 5325–5333. [[CrossRef](#)]
122. Casadebaigt, A.; Hugues, J.; Monceau, D. Influence of Microstructure and Surface Roughness on Oxidation Kinetics at 500–600 °C of Ti–6Al–4V Alloy Fabricated by Additive Manufacturing. *Oxid. Met.* **2018**, *90*, 633–648. [[CrossRef](#)]
123. Vvedenskii, A.V.; Grushevskaya, S.N. Kinetic peculiarities of anodic dissolution of copper and its gold alloys accompanied by the formation of insoluble Cu(I) products. *Corros. Sci.* **2003**, *45*, 2391–2413. [[CrossRef](#)]
124. Schultze, J.W.; Lohrengel, M.M.; Ross, D. Nucleation and growth of anodic oxide films. *Electrochim. Acta* **1983**, *28*, 973–984. [[CrossRef](#)]
125. Gu, J.-L.; Lu, S.-Y.; Shao, Y.; Yao, K.-F. Segregating the homogeneous passive film and understanding the passivation mechanism of Ti-based metallic glasses. *Corros. Sci.* **2021**, *178*, 109078. [[CrossRef](#)]
126. Macdonald, D.D. The Point Defect Model for the Passive State. *J. Electrochem. Soc.* **1992**, *139*, 3434–3449. [[CrossRef](#)]
127. Murr, L.E.; Esquivel, E.V.; Quinones, S.A.; Gaytan, S.M.; Lopez, M.I.; Martinez, E.Y.; Medina, F.; Hernandez, D.H.; Martinez, E.; Martinez, J.L.; et al. Microstructures and mechanical properties of electron beam-rapid manufactured Ti–6Al–4V biomedical prototypes compared to wrought Ti–6Al–4V. *Mater. Charact.* **2009**, *60*, 96–105. [[CrossRef](#)]
128. Shahsavari, M.; Imani, A.; Setavoraphan, A.; Schaller, R.F.; Asselin, E. Electron beam surface remelting enhanced corrosion resistance of additively manufactured Ti-6Al-4V as a potential in-situ re-finishing technique. *Sci. Rep.* **2022**, *12*, 11589. [[CrossRef](#)] [[PubMed](#)]
129. Schaller, R.F.; Mishra, A.; Rodelas, J.M.; Taylor, J.M.; Schindelholz, E.J. The Role of Microstructure and Surface Finish on the Corrosion of Selective Laser Melted 304L. *J. Electrochem. Soc.* **2018**, *165*, C234–C242. [[CrossRef](#)]
130. Heer, B.; Bandyopadhyay, A. Silica coated titanium using Laser Engineered Net Shaping for enhanced wear resistance. *Addit. Manuf.* **2018**, *23*, 303–311. [[CrossRef](#)]
131. Das, M.; Balla, V.K.; Kumar, T.S.S.; Bandyopadhyay, A.; Manna, I. Tribological, electrochemical and in vitro biocompatibility properties of SiC reinforced composite coatings. *Mater. Des.* **2016**, *95*, 510–517. [[CrossRef](#)]
132. Sezer, N.; Evis, Z.; Koç, M. Additive manufacturing of biodegradable magnesium implants and scaffolds: Review of the recent advances and research trends. *J. Magnes. Alloys* **2021**, *9*, 392–415. [[CrossRef](#)]
133. Putra, N.E.; Mirzaali, M.J.; Apachitei, I.; Zhou, J.; Zadpoor, A.A. Multi-material additive manufacturing technologies for Ti-, Mg-, and Fe-based biomaterials for bone substitution. *Acta Biomater.* **2020**, *109*, 1–20. [[CrossRef](#)]
134. Zhang, T.; Wang, W.; Liu, J.; Wang, L.; Tang, Y.; Wang, K. A review on magnesium alloys for biomedical applications. *Front. Bioeng. Biotechnol.* **2022**, *10*, 953344. [[CrossRef](#)]
135. Sillekens, W.H.; Bormann, D. Biomedical applications of magnesium alloys. In *Advances in Wrought Magnesium Alloys*; Elsevier: Amsterdam, The Netherlands, 2012; pp. 427–454.
136. Esmaily, M.; Zeng, Z.; Mortazavi, A.N.; Gullino, A.; Choudhary, S.; Derra, T.; Benn, F.; D’Elia, F.; Müther, M.; Thomas, S.; et al. A detailed microstructural and corrosion analysis of magnesium alloy WE43 manufactured by selective laser melting. *Addit. Manuf.* **2020**, *35*, 101321. [[CrossRef](#)]

137. Lovašiová, P.; Lovaši, T.; Kubásek, J.; Jablonská, E.; Msallamová, Š.; Michalcová, A.; Vojtěch, D.; Suchý, J.; Koutný, D.; Ghassan Hamed Alzubi, E. Biodegradable WE43 Magnesium Alloy Produced by Selective Laser Melting: Mechanical Properties, Corrosion Behavior, and In-Vitro Cytotoxicity. *Metals* **2022**, *12*, 469. [[CrossRef](#)]
138. Dong, J.; Tümer, N.; Putra, N.E.; Zhu, J.; Li, Y.; Leeftang, M.A.; Taheri, P.; Fratila-Apachitei, L.E.; Mol, J.M.C.; Zadpoor, A.A.; et al. Extrusion-based 3D printed magnesium scaffolds with multifunctional MgF 2 and MgF 2 –CaP coatings. *Biomater. Sci.* **2021**, *9*, 7159–7182. [[CrossRef](#)] [[PubMed](#)]
139. Li, Y.; Zhou, J.; Pavanram, P.; Leeftang, M.A.; Fockaert, L.I.; Pouran, B.; Tümer, N.; Schröder, K.-U.; Mol, J.M.C.; Weinans, H.; et al. Additively manufactured biodegradable porous magnesium. *Acta Biomater.* **2018**, *67*, 378–392. [[CrossRef](#)] [[PubMed](#)]
140. Salehi, M.; Maleksaedi, S.; Nai, M.L.S.; Gupta, M. Towards additive manufacturing of magnesium alloys through integration of binderless 3D printing and rapid microwave sintering. *Addit. Manuf.* **2019**, *29*, 100790. [[CrossRef](#)]
141. Prause, E.; Hey, J.; Beuer, F.; Schmidt, F. Wear resistance of 3D-printed materials: A systematic review. *Dent. Rev.* **2022**, *2*, 100051. [[CrossRef](#)]
142. Trelewicz, J.R.; Halada, G.P.; Donaldson, O.K.; Manogharan, G. Microstructure and Corrosion Resistance of Laser Additively Manufactured 316L Stainless Steel. *JOM* **2016**, *68*, 850–859. [[CrossRef](#)]
143. Ko, G.; Kim, W.; Kwon, K.; Lee, T.-K. The Corrosion of Stainless Steel Made by Additive Manufacturing: A Review. *Metals* **2021**, *11*, 516. [[CrossRef](#)]
144. Wang, L.; Tieu, A.K.; Lu, S.; Jamali, S.; Hai, G.; Zhu, Q.; Nguyen, H.H.; Cui, S. Sliding wear behavior and electrochemical properties of binder jet additively manufactured 316SS /bronze composites in marine environment. *Tribol. Int.* **2021**, *156*, 106810. [[CrossRef](#)]
145. Sánchez de Rojas Candela, C.; Riquelme, A.; Rodrigo, P.; Torres, B.; Rams, J. Wear behavior of additively manufactured 316L/SiCp composites with up to 60 wt% SiCp. *Ceram. Int.* **2022**, *48*, 33736–33750. [[CrossRef](#)]
146. Tonolini, P.; Marchini, L.; Montesano, L.; Gelfi, M.; Pola, A. Wear and corrosion behavior of 18Ni-300 maraging steel produced by laser-based powder bed fusion and conventional route. *Procedia Struct. Integr.* **2022**, *42*, 821–829. [[CrossRef](#)]
147. Sander, G.; Tan, J.; Balan, P.; Gharbi, O.; Feenstra, D.R.; Singer, L.; Thomas, S.; Kelly, R.G.; Scully, J.R.; Birbilis, N. Corrosion of Additively Manufactured Alloys: A Review. *Corrosion* **2018**, *74*, 1318–1350. [[CrossRef](#)]
148. Renner, P.; Jha, S.; Chen, Y.; Raut, A.; Mehta, S.G.; Liang, H. A Review on Corrosion and Wear of Additively Manufactured Alloys. *J. Tribol.* **2021**, *143*, 050802. [[CrossRef](#)]
149. Gil, F.J.; Planell, J.A. Shape memory alloys for medical applications. *Proc. Inst. Mech. Eng. Part H J. Eng. Med.* **1998**, *212*, 473–488. [[CrossRef](#)] [[PubMed](#)]
150. Yuan, B.; Zhu, M.; Chung, C.Y. Biomedical Porous Shape Memory Alloys for Hard-Tissue Replacement Materials. *Materials* **2018**, *11*, 1716. [[CrossRef](#)] [[PubMed](#)]
151. Petrini, L.; Migliavacca, F. Biomedical Applications of Shape Memory Alloys. *J. Metall.* **2011**, *2011*, 501483. [[CrossRef](#)]
152. Ebrahimi, M.; Attarilar, S.; Gode, C.; Kandavalli, S.R.; Shamsborhan, M.; Wang, Q. Conceptual Analysis on Severe Plastic Deformation Processes of Shape Memory Alloys: Mechanical Properties and Microstructure Characterization. *Metals* **2023**, *13*, 447. [[CrossRef](#)]
153. Buciumeanu, M.; Bagheri, A.; Silva, F.S.; Henriques, B.; Lasagni, A.F.; Shamsaei, N. Tribocorrosion Behavior of NiTi Biomedical Alloy Processed by an Additive Manufacturing Laser Beam Directed Energy Deposition Technique. *Materials* **2022**, *15*, 691. [[CrossRef](#)]
154. Ma, L.; Li, W.; Yang, Y.; Ma, Y.; Luo, K.; Jia, B.; Xu, Z.; Yu, Z. Corrosion Behavior of NiTi Alloys Fabricate by Selective Laser Melting Subjected to Femtosecond Laser Shock Peening. *Coatings* **2021**, *11*, 1078. [[CrossRef](#)]
155. Zhang, L.; Ren, D.; Ji, H.; Ma, A.; Daniel, E.F.; Li, S.; Jin, W.; Zheng, Y. Study on the corrosion behavior of NiTi shape memory alloys fabricated by electron beam melting. *npj Mater. Degrad.* **2022**, *6*, 79. [[CrossRef](#)]
156. Lu, B.; Cui, X.; Jin, G.; Dong, M.; Fang, Y.; Wen, X.; Ma, W. Effect of La2O3 addition on mechanical properties and wear behaviour of NiTi alloy fabricated by direct metal deposition. *Opt. Laser Technol.* **2020**, *129*, 106290. [[CrossRef](#)]
157. Liu, G.; Zhou, S.; Lin, P.; Zong, X.; Chen, Z.; Zhang, Z.; Ren, L. Analysis of microstructure, mechanical properties, and wear performance of NiTi alloy fabricated by cold metal transfer based wire arc additive manufacturing. *J. Mater. Res. Technol.* **2022**, *20*, 246–259. [[CrossRef](#)]
158. Pepelnjak, T.; Stojšić, J.; Sevšek, L.; Movrin, D.; Milutinović, M. Influence of Process Parameters on the Characteristics of Additively Manufactured Parts Made from Advanced Biopolymers. *Polymers* **2023**, *15*, 716. [[CrossRef](#)] [[PubMed](#)]
159. Gor, M.; Soni, H.; Wankhede, V.; Sahlot, P.; Grzelak, K.; Szachgluchowicz, I.; Kluczyński, J. A Critical Review on Effect of Process Parameters on Mechanical and Microstructural Properties of Powder-Bed Fusion Additive Manufacturing of SS316L. *Materials* **2021**, *14*, 6527. [[CrossRef](#)] [[PubMed](#)]
160. Kong, D.; Dong, C.; Ni, X.; Li, X. Corrosion of metallic materials fabricated by selective laser melting. *npj Mater. Degrad.* **2019**, *3*, 24. [[CrossRef](#)]

Disclaimer/Publisher’s Note: The statements, opinions and data contained in all publications are solely those of the individual author(s) and contributor(s) and not of MDPI and/or the editor(s). MDPI and/or the editor(s) disclaim responsibility for any injury to people or property resulting from any ideas, methods, instructions or products referred to in the content.